npj | natural hazards

Article

https://doi.org/10.1038/s44304-026-00203-w

Global urban exposure near volcanoes is increasing: a spatio-temporal analysis from 1975 to 2030

Check for updates

Elinor S. Meredith[1,2] ✉, Rui Xue Natalie Teng[1] ✉, Susanna F. Jenkins[1], Eleanor M. Tennant[3], David Lallemant[1], Josh L. Hayes[4] & Sébastien Biass[5]

Urban populations are increasingly moving into hazardous areas, which leads to widespread and frequent impacts from hazard events. Although these exposure trends have been quantified for other hazards, global exposure analyses for volcanic hazards remain limited. Here, we quantify global and regional changes in city exposure to volcanic hazards through time. With GHS-UCDB and GHS-POP datasets, we use spatio-temporal metrics to track urban expansion within 100 km of volcanoes active in the Holocene from 1975 to 2020, with projections to 2030. The number of cities within 100 km of volcanoes is projected to more than double, with populations increasing by 154%. The proportion of people within 100 km of volcanoes who live in cities increases from 44% (~186 million) in 1975 to over 50% by 2030 (~473 million). Exposed city populations concentrate within 20–30 km from volcanoes, and average urban population density generally decreases closer to volcanoes. Exposure growth is highest in Southeast Asia and East Africa. Most cities expand and densify, with many growing faster toward nearby volcanoes. Case studies show how urban expansion intersects with volcanic impact pathways. These trends indicate that urban expansion is amplifying volcanic risk and highlight the need to integrate hazard data into urban planning.

By 2050, almost 70% of the world's population will live in cities[1]. Population growth and land scarcity are driving urban expansion into areas exposed to natural hazards[2–5]. As a result, disasters are becoming increasingly likely to affect urban areas. Global disaster loss data confirm that urban populations account for a rising share of disaster impacts, and this trend is expected to increase[6].

Tracking and projecting the exposure of cities through time can help to identify areas with the fastest growth rates, in order to focus more targeted localised research and mitigation efforts. Past studies have provided insights into urban growth rates in hazard-prone areas on varying scales, such as for flooding[3,5,7–10], landslides[11–13], and earthquakes[10,14,15]. These temporal exposure studies and datasets have supported localised efforts to implement hazard mitigation or update building codes, enhancing urban resilience in areas exposed to natural hazards (e.g., Mohuya et al.[16], Muis et al.[17], Asian Development Bank[18]).

With dense concentrations of populations, buildings, and infrastructure, cities are particularly susceptible to the effects of disasters caused by natural hazards[19,20]. Despite rapid population growth around volcanoes[21,22], and the increasing vulnerability of cities to volcanic hazards[23–26], quantitative assessments of urban exposure to volcanic hazards remain limited and often static in time (e.g., Meredith et al.[27]). Ongoing unrest at Campi Flegrei, a caldera underlying the densely populated city of Naples, Italy, is one example of these challenges. The recent seismic activity and ground deformation have prompted extensive monitoring and preparedness initiatives, with risk assessments and evacuation planning being further developed[28,29]. Past examples of impacts at other locations highlight the severity of such threats, for instance the 2002 and 2021 lava flows of Nyiragongo devastated Goma, Democratic Republic of Congo, with destruction of health centres, schools, power supply, thousands of homes displacing residents, and critical infrastructure such as water tanks in the city, depriving half a million people of access to water[30–32]. Similarly, the 1991 eruption of Mount Pinatubo devastated Central Luzon, the Philippines, including the city of Angeles and the Clark Air Base, displacing hundreds of thousands of residents[33,34]. The disruption extended nationally with lahars

[1]Earth Observatory of Singapore, Asian School of the Environment, Nanyang Technological University, Nanyang, Singapore. [2]Faculty of Geo-Information Science and Earth Observation (ITC), University of Twente, Enschede, the Netherlands. [3]Earth Observatory of Singapore @ NTU, Interdisciplinary Graduate Programme, Nanyang Technological University, Nanyang, Singapore. [4]Earth Sciences New Zealand, Lower Hutt, New Zealand. [5]Department of Earth Sciences, University of Geneva, Geneva, Switzerland. ✉e-mail: elinorsi001@e.ntu.edu.sg; natalie.tengrx@ntu.edu.sg

and tephra fall that damaged agricultural production, contributing to food insecurity, while the economic burden and loss of infrastructure had long-term effects on the Philippines' GDP[35]. While the impacts of volcanic eruptions on cities are severe, the cities' roles as political and economic hubs[36], and the dependence and interconnectedness of infrastructure[37], mean that impacts can also have widespread cascading consequences across the city, nation, and region.

On a global scale, Meredith et al.[27] identified more than 1133 cities worldwide exposed to volcanic hazards using 2020 population data, ranking Jakarta, Bandung (Indonesia), and Naples (Italy) as the most exposed cities within 100, 30, and 10 km from volcanoes active in the Holocene, respectively. Several studies have examined temporal changes in population exposure to volcanic hazards, including global and regional analyses of population distribution near volcanoes (e.g., Small & Naumann[22]; Freire et al.[21]; Strader et al.[38]). However, these assessments do not show how city expansion can redistribute exposure. Earlier global studies also sought to identify key exposed cities, such as Chester et al.[25], Heiken[24], and Auker et al.[39]. These studies provided perspectives on urban exposure to volcanic hazards, but did not quantify how cities and their populations evolve through time in relation to nearby volcanoes.

Regional analyses have been conducted, for example, Jenkins et al.[40] on relative tephra fall hazard in Asia, and Strader et al.[38] who examined volcanic hazard population exposure in the Pacific Northwest from 1940 to 2100. Jenkins et al.[41] extended this approach using building, infrastructure, agriculture, and population datasets from 2019 and 2020 to quantify exposure to volcanic hazards in Southeast Asia. City-level studies provide local insights into how volcanic hazards intersect with urban areas, such as in Naples[42], Arequipa[43], Auckland[44], and communities around Mount Rainier[45]. Despite these efforts, the lack of integrated and temporal global datasets linking urban change with volcanic hazards limits our ability to track and forecast exposure trajectories. Comparing volcanic hazard distribution with both historical and projected urban expansion is essential for assessing evolving volcanic risk. Although city expansion is shaped by a range of drivers, these factors cannot be reliably inferred at a global scale. Local examples can illustrate some contextual differences.

Global and regional assessments of population exposure to volcanic hazards commonly use concentric buffers of varying radii around volcanoes to estimate exposure levels (e.g., Freire et al.[21], Meredith et al.[27], Small & Naumann[22]). The choice of the radii distances is based on past observations of the average maximum extents of life-threatening volcanic hazards at different eruption magnitudes measured by the Volcanic Explosivity Index (VEI)[46]. For instance, VEI ≤ 3 eruptions typically affect areas within ~10 km, VEI ≤ 4 eruptions up to ~30 km, and VEI ≤ 5 eruptions up to ~100 km[47,48]. This conservative approach allows for easy comparison between volcanoes and is useful for volcanoes where data for probabilistic hazard models are unavailable. The Population Exposure Index (PEI), developed by Aspinall et al.[49] and elaborated by Brown et al.[50] weights these population exposure counts by area of the buffers and probability of impact based on the average distance of past fatalities. However, this approach does not fully capture the spatial gradient in population density, particularly between 30 and 100 km away from volcanoes, where large urban areas are predominantly located[27]. Biass et al.[48] evaluated the accuracy of assessing exposure by radii against detailed hazard footprints, while Nieto-Torres et al.[51] proposed inclusive volcanic risk rankings that account for exposure beyond simple distance measures. Using more intervals between these radii distances, and considering the directionality of the spreading, may be useful to assess more subtle changes in population density distribution around volcanoes, and aligns with these calls to refine methodologies to better couple hazard footprints with exposure.

In this study, we analyse urban expansion near 1264 volcanoes active in the Holocene (last ~11,000 years) using a range of spatial and demographic indicators across global, regional, and city scales. Our study focuses on the exposure of city populations, looking at the presence of people in potentially hazardous areas, rather than on volcanic risk, which also depends on vulnerability. This enables us to examine how changes in city spatial extent and density modify urban population exposure over time, which often coincide with dense concentrations of buildings and infrastructure. By analysing population and urban land area data spanning from 1975 to 2020, along with future projections for 2025 and 2030, we map and assess the evolving spatio-temporal trends of city exposure to volcanic hazards. Using key spatio-temporal indicators, we identify cities experiencing the most rapid exposure growth, particularly those expanding towards nearby volcanoes. Specifically, we quantify global and regional changes in city population and area within defined distances of volcanoes active in the Holocene from 1975 to 2030. We select nine case study cities to illustrate local-scale examples of city exposure growth related to hazard paths and to contextualise the global exposure trends at the local scale. Our findings provide valuable evidence for policymakers to prioritise volcanic risk preparedness and mitigation in urban planning, for example, through land use zoning and establishing exclusion zones.

Results

To evaluate patterns of urban development near volcanoes, we compiled and analysed a global dataset of cities and their populations exposed to volcanic hazards over time. The results presented below describe changes in urban extent, population distribution, and exposure within proximity buffers, first at global and regional scales using 10-km ring buffers to 100 km, and then at the city level using 10-, 30-, and 100-km cumulative buffers. Finally, we present nine case studies that illustrate localised patterns of exposure and expansion near volcanic hazard paths.

Globally and regionally, city exposure is increasing

Currently, there are ~853 million people living within 100 km of 598 Holocene volcanoes around the world (Fig. 1), with 50% of these living in cities (430 M; Table 1). On average, within 100 km of volcanoes, each 5-year interval shows an increase of ~26 million people living in cities, compared with ~19 million people living outside cities. As a result, the proportion of the population living in cities within 100 km of Holocene volcanoes rose from 44% in 1975 to exceed the non-urban population in 2005, reaching a projected 52% by 2030 (Table 1).

Between 1975 and 2030, the number of cities located within 100 km of Holocene volcanoes will increase by 106% from 582 to 1196 (Fig. 2A). Over the same period, the population living in these exposed cities is expected to grow by 154%, from 186 million to 473 million people (Table 1 and Fig. 2C). Southeast and East Asia account for the largest proportion of exposure each year (Fig. 2B, D). While the proportion of exposed city population is generally even across the years for each continent, it is decreasing in Europe and East Asia, and the proportion is increasing in Mexico and Central America (Fig. 2D). African regions show the largest increases in both exposed city counts and city population from 1975 to 2030 (Fig. 2B, D).

Population density increases with distance from Holocene volcanoes

City populations are not evenly distributed across the 10-km distance ring buffers surrounding Holocene volcanoes. Globally, the highest number of the city population remains located within 20–30 km from volcanoes, which rose ~150% from ~24.6 million people in 1975 to ~61.8 million people in 2030 (Fig. 3A). Fig. 3 shows a steady increase in city populations globally through time, and city populations within 10 km of volcanoes remain the lowest.

The distribution of city populations across the buffers varies by region. The greatest total exposure of people is between 40–50 km from volcanoes in Southeast Asia (26.04 million people in 2020), 55% of the global total in that buffer (47.69 million). For Southeast Asia, this 40–50 km buffer also represents the largest growth in city populations, from 9.97 million in 1975 to 29.91 million in 2030 (Fig. 3B). In North America, dominated by the USA, city populations peak at 60–80 km from volcanoes (Fig. 3C) and only projected city populations are within 40 km (Fig. 3C). Although total city populations near volcanoes there are an order of magnitude lower than in Southeast Asia, dominated by Indonesia, growth appears much greater with

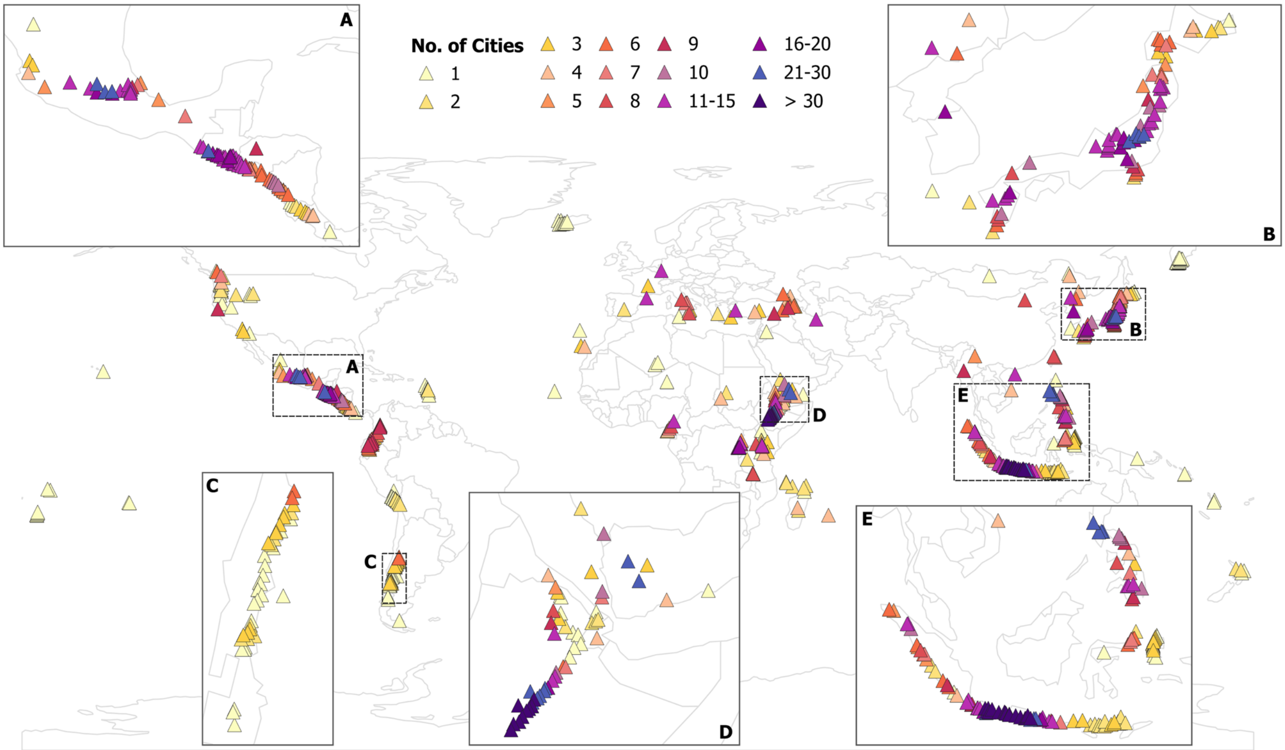

Fig. 1 | Spatial distribution of volcanoes near cities. The 598 volcanoes (triangles) within 100 km of a city are coloured by the maximum number of cities within 100 km between 1975 and 2030 (projected) from least (light yellow) to most (dark blue). Map insets are included for parts of **A**) Mexico and Central America, **B**) East Asia, **C**) South America, **D**) East Africa, and **E**) Southeast Asia.

Table 1 | Global numbers of populations within 100 km from Holocene volcanoes from 1975 to 2030, taken from GHS-POP data, with the number and proportion of those populations located within the city polygons

Year	Number of cities	Population < 100 km of volcanoes			
		In total (M)	In cities (M)	Outside of cities (M)	% in cities
1975	582	425.45	186.14	239.31	43.75
1980	633	472.72	212.63	260.09	44.98
1985	692	520.3	238.76	281.54	45.89
1990	743	569.43	266.79	302.64	46.85
1995	835	614.57	298.03	316.54	48.49
2000	927	660.86	327.78	333.08	49.6
2005	1007	705.43	355.5	349.93	50.39
2010	1073	751.51	382.92	368.59	50.95
2015	1124	797.95	410.18	387.77	51.4
2020	1129	852.99	430.35	422.64	50.45
2025	1158	879.85	450.33	429.52	51.18
2030	1196	918.02	473.26	444.76	51.55

Note that 2025 and 2030 are using projected data.

city population increasing in the 70–80 km distance from volcanoes by around seven times, from nearly 339,000 in 1975 to 2.52 million in 2030 (Fig. 3C). In Mexico and Central America, the largest populations are within 20–30 km from volcanoes with 13.40 million projected for 2030, a near tripling in exposed populations since 5.65 million in 1975 (Fig. 3D). In East Asia, dominated by Japan, and East Africa, dominated by Ethiopia, populations are more dispersed, with more city populations concentrated farther away from volcanoes than in other regions (Fig. 3E, F). Most city populations are located in the 80–90 km buffer in East Asia, with overall more gradual increases through time compared to other regions, from 11.85 million in 1975 to 16.34 million in 2030 (Supplementary Data 1).

The density of these populations within city areas increases globally through time (Fig. 4A). On average, city population density increases steadily by ~1000 people/km^2 between 1975 and 2030. However, this growth varies by distance from volcanoes. Globally, populations located farther away from volcanoes generally exhibit higher densities and a greater density increase through time than those located closer to volcanoes (Fig. 4A). Since 2000, the greatest city population density is located between 70 and 80 km from volcanoes. In contrast, city populations within 10 km of volcanoes maintain the lowest average densities throughout the time period. These trends indicate that cities across all distances have grown denser over time, while city areas farther from volcanoes concentrate more population per unit area than those closer to volcanoes.

Trends in city population density growth differ from region to region. In Mexico and Central America, most distance buffers experienced city population density growth from 1975 to 2000, followed by a plateau or decline in the years following (Fig. 4B). Here, generally the distance buffers closer to volcanoes have higher city population densities compared to those farther away (Fig. 4B). In Southeast Asia, average population density was more stable through time, with some initial decline in the 1980s, followed by gradual increase after 2000 (Fig. 4C).

Growth trends of cities near Holocene volcanoes

Across the 1137 cities exposed to volcanic hazards in 2030 used for growth analysis, the majority have experienced expansion and/or densification, observed across cumulative distance buffers (10-, 30-, and 100-km buffers). Within these different cumulative distance buffers, there are 94 cities located partially or fully within 10 km of Holocene volcanoes and 384 cities partially or fully within 30 km by 2030. Based on the 1,137 cities, 85% ($n = 962$) of cities expanded, and 59% ($n = 666$) of cities densified their exposed area, in

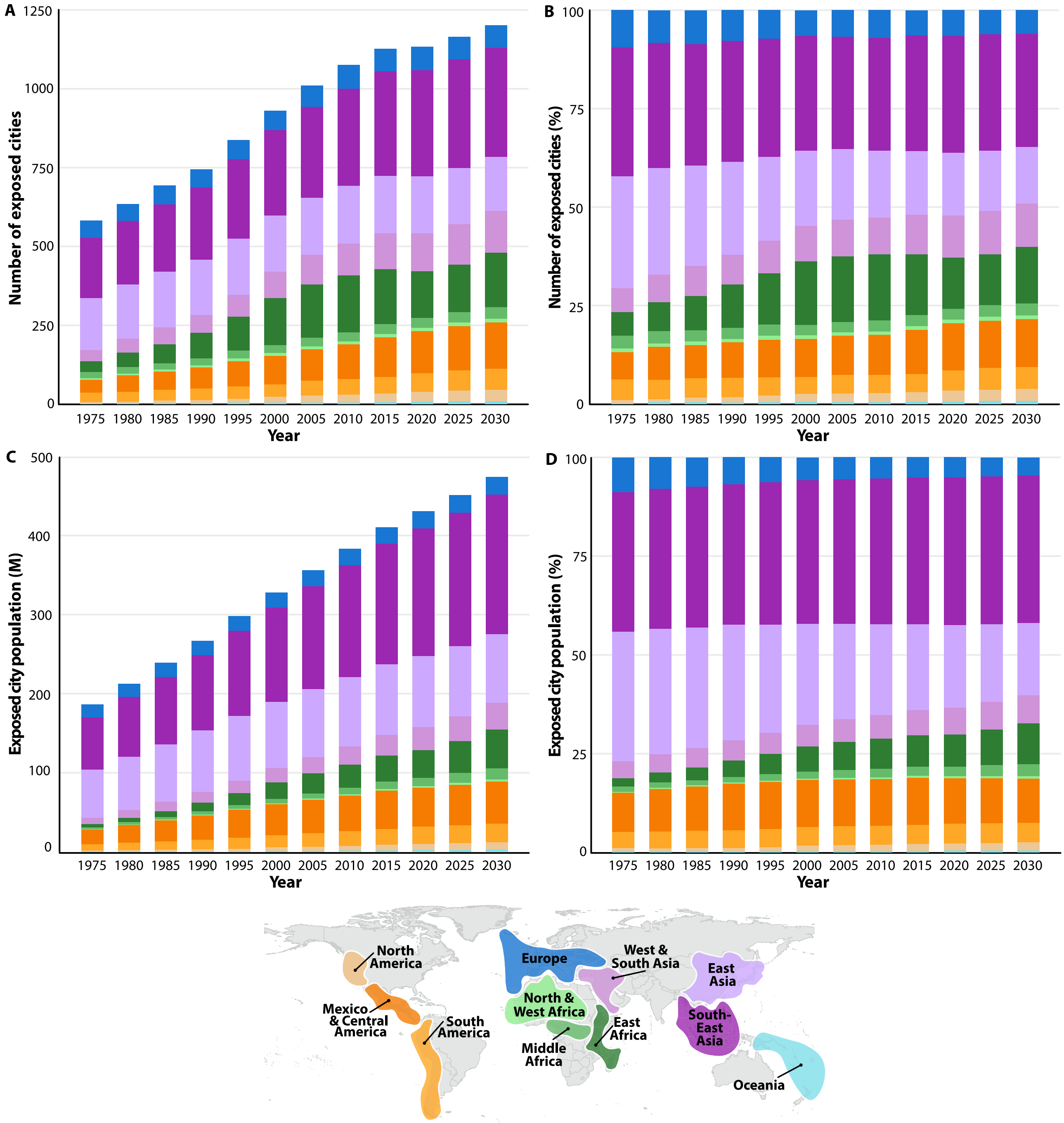

Fig. 2 | Temporal trends in urban exposure to Holocene volcanoes from 1975 to 2030. City exposure trends presented as **A**) stacked and **B**) normalised number of exposed cities within 100 km of a Holocene volcano, and **C**) stacked and **D**) normalised exposed city population in millions for the same set of cities and distance threshold. Coloured by subregion. Both city and population numbers show steady increases over time, with the largest contributions consistently from Southeast Asia and East Asia.

at least one five-year period. The proportion of cities that experienced expansion and densification are similar in each buffer (Fig. 5A, B). City area expansion appears to be episodic, with most cities having an increase in exposed area 25-50% of the time since it was first exposed (Fig. 5C). Whilst few cities increase their area exposure in every 5-year period, their exposure can still increase through densification of existing city areas.

Cities are situated either partially or fully within the 0–10, 10–30, and 30–100 km distance buffers around Holocene volcanoes (Supplementary Data 3), and only ten cities span across all three distance buffer boundaries (Fig. 6). All cities have expanded their footprints within distance buffers over time, but patterns differ between absolute growth and proportional growth, and between area and population exposure (Fig. 6). The largest *absolute* exposed city populations and areas are between 30 and 100 km from volcanoes, mostly in Jakarta (1707 km^2 to 3397 km^2), Manila (1066 km^2 to 2300 km^2), and Mexico City (1088 km^2 to 1398 km^2). Jakarta's total exposed area more than doubles (2110 km^2 to 4700 km^2), the highest of any city. Although Taipei (74 km^2 to 398 km^2) has a similar relative increase in exposed area to Mexico City at 30–100 km, Mexico City's exposed population is substantially larger (within 100 km in 2030: Mexico City, ~18 million; Taipei, ~10 million). There is greater *relative* area and population growth generally closer to volcanoes, such as Surabaya, which nearly doubles its exposed area within both 0–10 (62 km^2 to 101 km^2) and 10–30 km

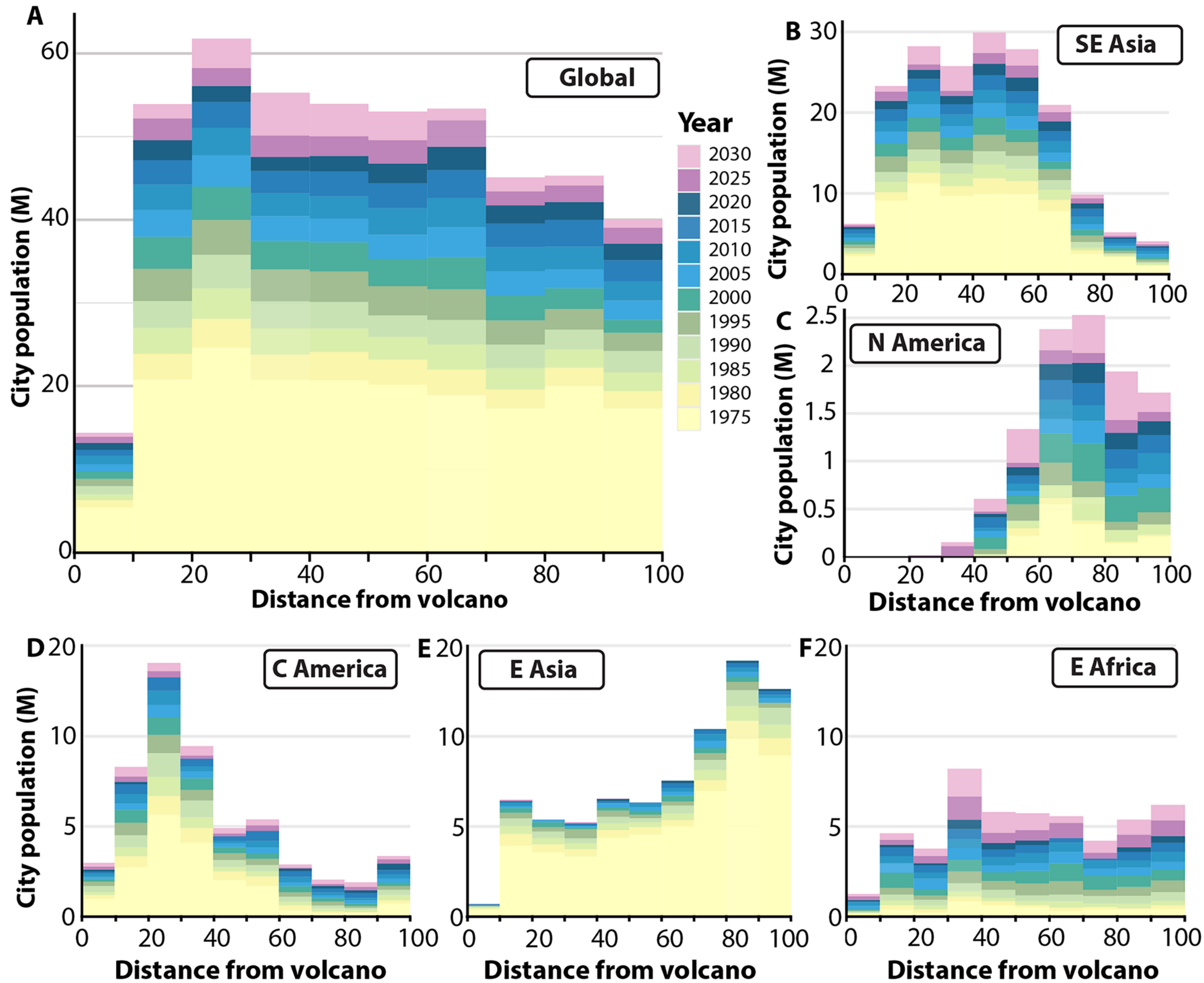

Fig. 3 | Spread of populations around Holocene volcanoes. City population coloured by year for **A**) global, and subregions: **B**) Southeast Asia, **C**) North America, **D**) Mexico and Central America, **E**) Eastern Asia, and **F**) East Africa. Colours represent decades from 1975 (lightest) to 2020 (darkest), and projections to 2030 are shown in purple, showing temporal change in city populations with distance from volcanoes. Note the y-scales are different for each plot.

(332 km^2 to 761 km^2), while expanding by slightly less than 50% at 30–100 km (303 km^2 to 427 km^2).

For the 270 cities that span across at least two of the <10, 10–30, or 30–100 km distance buffers in 2030, city area growth can occur either in a closer or farther buffer from the volcano, which will either increase or decrease the city's proportional exposure to volcanic hazards (Fig. 7). For a given city, if there was no preferential growth towards volcanoes, the proportion of the city within each buffer should remain constant through time. Across all the cities, random growth would result in approximately equal numbers increasing and decreasing in exposed area. However, most cities fall above the lowest dashed line in Fig. 7, indicating that the proportion of city area within the buffers increases over time. The rate of growth in exposed areas relative to the total city growth is higher for more than half of the cities partially within 10 km of a volcano (58%, 43/74), whereas the proportions for the 30 km (50%, 60/120) and 100 km (45%, 39/87) buffers were close to the ~50% expected under no preferential growth. Major shifts in spatial expansion are indicated by large bubbles, and larger changes in population density are indicated by darker colour shades, indicating rapid and concentrated increases in exposed area (Fig. 7). Within the exposed areas of cities, population density trajectories vary, with some distance buffers becoming increasingly crowded, while others retain low densities.

Key examples of city exposure expansion towards volcanic hazards

We find that, generally, cities are spreading towards volcanoes, which is moving dense concentrations of people and infrastructure into hazardous zones (Fig. 7). To explore this further, below we give details of nine key cities, most of which are capital cities and also rank highly in terms of different exposure and growth metrics to illustrate the complexities of urban growth which are further discussed in the Discussion. The high exposure and growth of key urban centres illustrate different patterns of urban expansion near volcanoes. Below, after volcano names, we provide years of the last recorded eruption if known, in parentheses, from the Global Volcanism Program. When we refer to volcanic flow directions as outputs of FlowDIR, these are for lava flows and dome collapse-derived block-and-ash flows from the volcanic summits.

Jakarta, Bandung, and Tarogong, Indonesia

Jakarta, Tarogong, and Bandung cities, located in West Java, show high rates of change in exposed area within 10 km and 30 km of multiple volcanoes. Globally, Jakarta has the largest population within 100 km of volcanoes (n = 38.5 million), overtaking Tokyo in 2005 (Fig. 8), whilst Bandung has the largest population living within 30 km of volcanoes (n = 9 million), overtaking Taipei and Mexico City in 2000 (Fig. 8). Jakarta is spreading along the

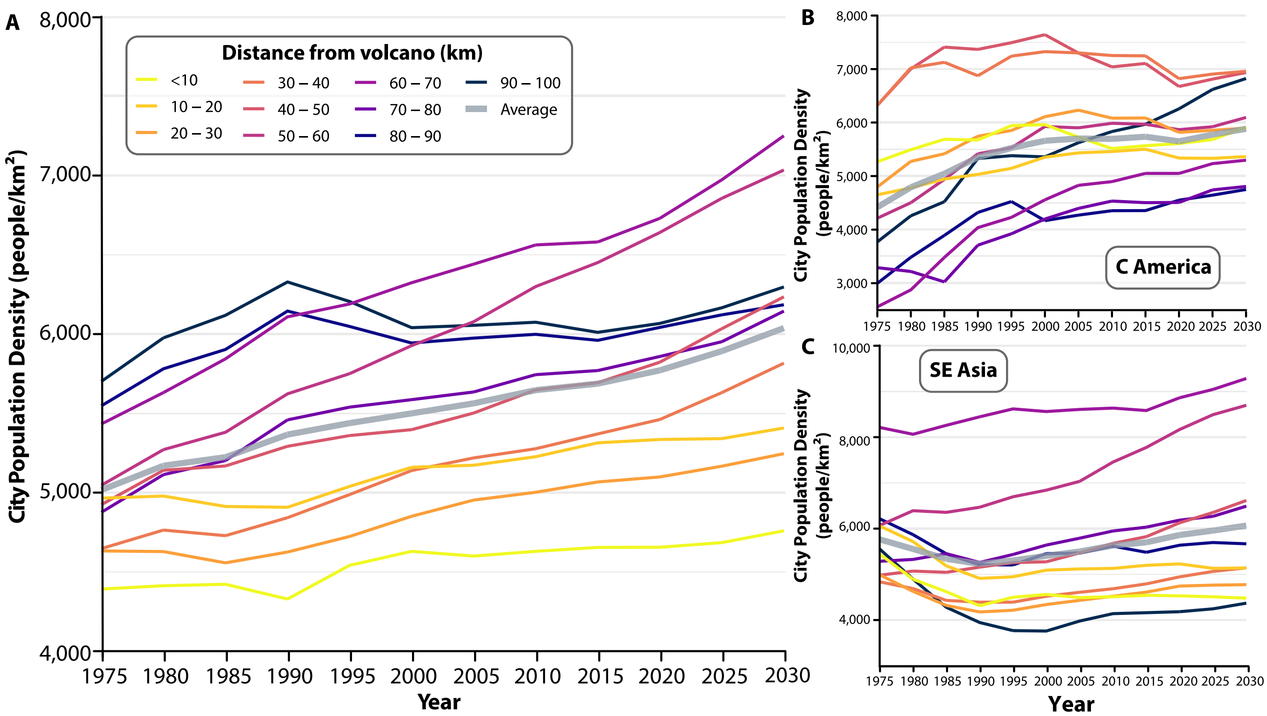

Fig. 4 | City population density through time. City population density is plotted from 1975 to 2030 (projected) for **A**) globally, and example subregions: **B**) Mexico and Central America and **C**) Southeast Asia. Each coloured line represents city population within a buffer distance from closest (<10 km, yellow) to farthest (dark blue, 90–100 km) from volcanoes. The grey lines show the average city population density across the ring buffers.

coastline at the north of Java, and the three cities are connected along highways (Fig. 9A).

Populations are exposed to tephra fall from volcanoes east of the cities due to prevailing westward wind (Fig. 9A). For volcanic flow hazards, areas of urban expansion in the south of Jakarta, and Cipanas, are exposed to flows from Gede volcano (1957), where likely travel directions are towards the north and northeast of the volcano and population exposure is within 10 km (Fig. 9A). To the west of Jakarta, flows from Karang are likely towards the west of the city, and towards the closer smaller city of Pandeglang, flows from Pulosari are directed away from Jakarta but towards the smaller city of Sukasari (Fig. 9A). Parts of Tarogong are located within 10 km of Guntur volcano (1847) (Fig. 9A). Papandayan (2002) and Galunggung (1984) volcanoes show highest probabilities of flows towards Tarogong (~11% and ~12%, respectively); (Fig. 9A). Future projections show a connection of Tarogong with the smaller city Hegarsari, which is also exposed to flows from Guntur volcano (Fig. 9A). Bandung and nearby Sumedang have exposure to flows from Tampomas in the northeast, with higher flow direction likelihoods in the direction of projected expansion (Fig. 9A). Other nearby volcanoes to these cities, such as Salak (1938), Pulosari, Karang, Tangkuban Perahu (2019), and Patuha are more likely to experience flows directed away from these key cities, although there are other city populations close by (Fig. 9A).

Addis Ababa, Ethiopia

Addis Ababa, the capital of Ethiopia, is highly ranked for preferential growth from the 30–100 km distance buffer into the 10–30 km distance buffer around volcanoes (Fig. 7). Exposed populations have gradually increased within all distance buffers until 2010, and rapidly increases since 2010 in the 10-km and 30–100 km distance buffers (Fig. 8). Located in the Ethiopian rift zone, city populations reside within 100 km of up to nine volcanoes, including Bishoftu Volcanic Field and Boset volcano to the southwest (Fig. 9B). Much of the city's recent expansion has occurred to the northeast of the city and along the road connecting Addis Ababa with Bishoftu (Fig. 9B).

Based on the prevailing wind directions, the city is exposed to tephra fall from nearby and distant volcanoes, particularly from volcanoes to the east of the city (Fig. 9B). Continued growth towards volcanoes increases the proximity of populations to potential flows.

Naples, Italy

Naples, on the west coast of Italy, lies exposed to three volcanoes: Vesuvius volcano (1944) to the east, Ischia volcano (1302) to the west, and Campi Flegrei caldera (1538), within which part of the city is located. Naples consistently has the largest population within 10 km of volcanoes (Fig. 8). The city surrounds Vesuvius, with its centre to the northeast of the volcano and the urban area extending south and east, with more recent development of city growth towards the north and northwest of the volcano.

Naples is exposed to tephra from all three volcanoes (Vesuvius, Campi Flegrei, and Ischia). Prevailing eastward wind suggests the southeastern areas of the city are particularly exposed to tephra fall (Fig. 9C). Volcanic flows from Vesuvius are more likely to be directed towards the south and west of the volcano, coinciding with areas of Naples, and not with San Giuseppe Vesuviano to the north.

San Salvador, El Salvador

San Salvador in 2020 was exposed to 25 volcanoes within 30 km[27] (Fig. 9). The city's population (1.67 million in 2020 in our dataset) has grown by ~70% since 1975 (0.97 million). The capital sits between and on the flanks of the San Salvador (1917) and Ilopango caldera (1880) volcanic complexes and has expanded northeast and southwest around them in the 1990s (Fig. 9D). There was a steep increase in population within 10 km of these volcanoes until 2000, with a gradual increase since (Fig. 8).

The city is exposed to tephra fall from the San Salvador volcano under prevailing winds (Fig. 9D). Expansion of the city on the flanks of the volcanoes places new development in areas likely to experience tephra fall. Tephra fall from the Ilopango Caldera, located east of the city, may also affect San Salvador city. Additional exposure comes from tephra carried

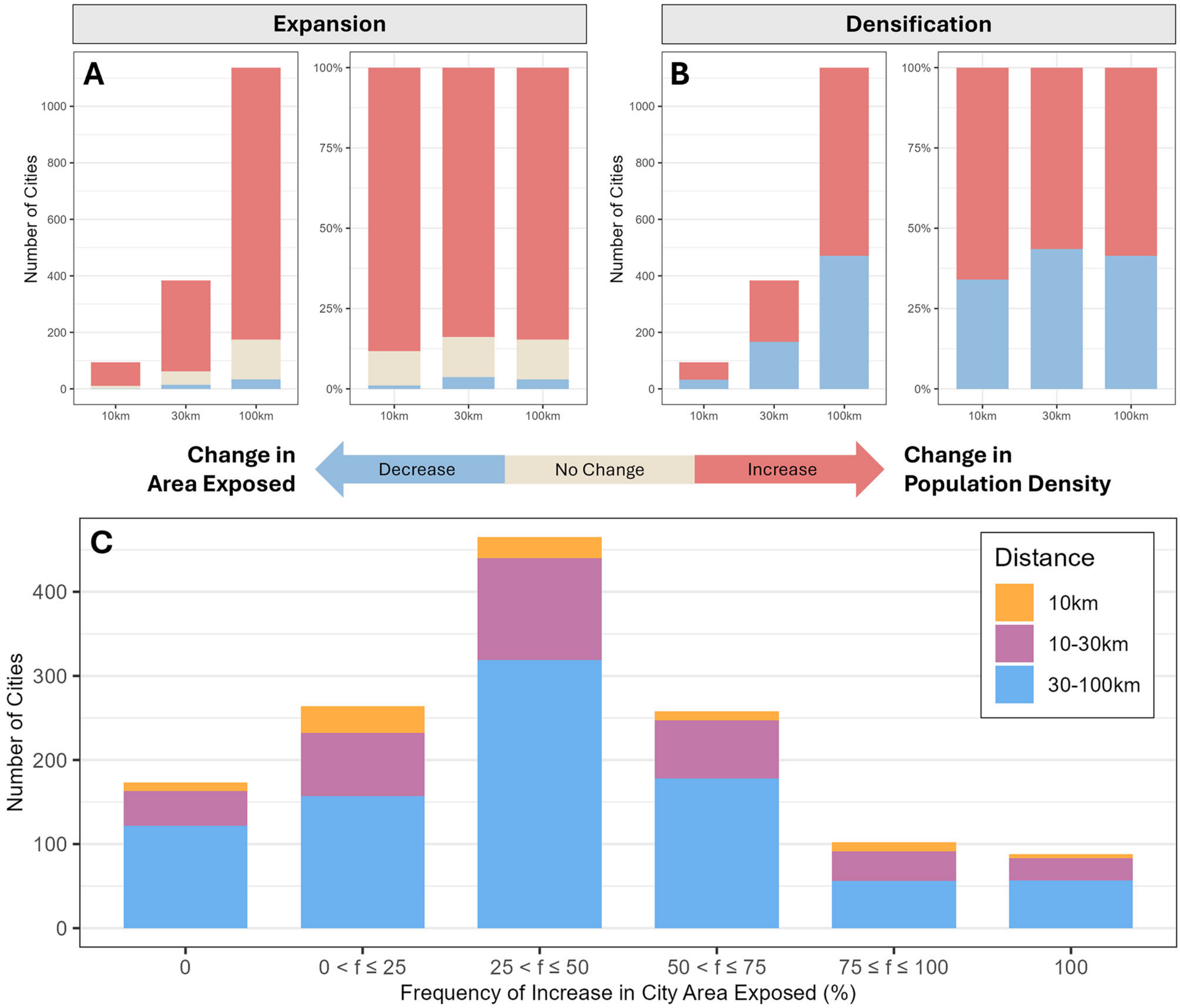

Fig. 5 | Overview of city growth for cities that are projected to be exposed in 2030 and at least one time period prior. Number and proportion of cities with changes in area exposed **A**) and population density **B**) within 10, 30, and 100 km of at least one volcano between the year the city was first exposed and projected values for 2030. **C**) Number of cities experiencing different frequencies of increase in city area between 0–10, 10–30, and 30–100 km from a volcano. The frequency metric is the proportion of 5-year periods where there was an increase in city area exposed between the year the city was first exposed and projected to 2030, expressed as a percentage.

from volcanoes to the west of the city and distant volcanoes, like San Miguel (2023)[52].

San Salvador is exposed to volcanic flow hazards[53,54]. The city is spreading to the north of Ilopango caldera (Fig. 9D). Flows from the San Salvador crater are more likely to be directed towards the northwest (Fig. 9D). This direction is away from San Salvador city centre, however the city of Lourdes lies within 10 km of San Salvador volcano towards the higher likelihood western flow direction (Fig. 9D). San Vicente volcano located southeast of San Salvador city has a most likely flow travel direction towards the city, although San Vicente is ~30 km from the city with Ilopango between (Fig. 9D).

Tokyo, Japan

Tokyo, the capital of Japan, located on the east of Honshu island, ranks second globally for the number of people exposed to volcanoes within 100 km in 2020 (n = 30 million), and was ranked highest until 2000 when it was overtaken by Jakarta (Fig. 8). The city's geographic spread shows a contrast between the northwest and southwest areas which are exposed to up to 16 volcanoes, including Fujisan (1708) and Hakoneyama (2015) to the southwest of the city, whilst the east of the city faces no volcanoes (Fig. 9E). Tokyo has recently spread slightly towards volcanoes in the north (Fig. 9E). Neighbouring cities to the northwest of Tokyo, such as Takasaki, exhibit exposure to up to 13 volcanoes (Fig. 9E).

Tokyo is exposed to tephra fall from nearby volcanoes such as Fujisan and Hakoneyama volcanoes, with prevailing winds blowing eastward (Fig. 9E). Growth northward and westward increases the residents' exposure to potential tephra fall. Our analysis suggests that flows from Hakoneyama are more likely to be directed northwest towards Fujisan and away from Tokyo, reducing direct exposure of the city, though some surrounding developments remain within possible flow directions (Fig. 9E).

Quito, Ecuador

Populations in Quito, the capital of Ecuador, live within 100 km of up to 16 volcanoes. The city is highly ranked for population within all three buffers (Fig. 8), and ranked highly for preferential growth into the 10 km zone near volcanoes (Fig. 7). Quito's recent expansion has occurred mostly in the south, expanding towards Atacazo volcano (320 BCE), towards the north and Pululahua volcano (290 CE), and slightly westward towards Guagua Pichincha volcano (2002; Fig. 9F).

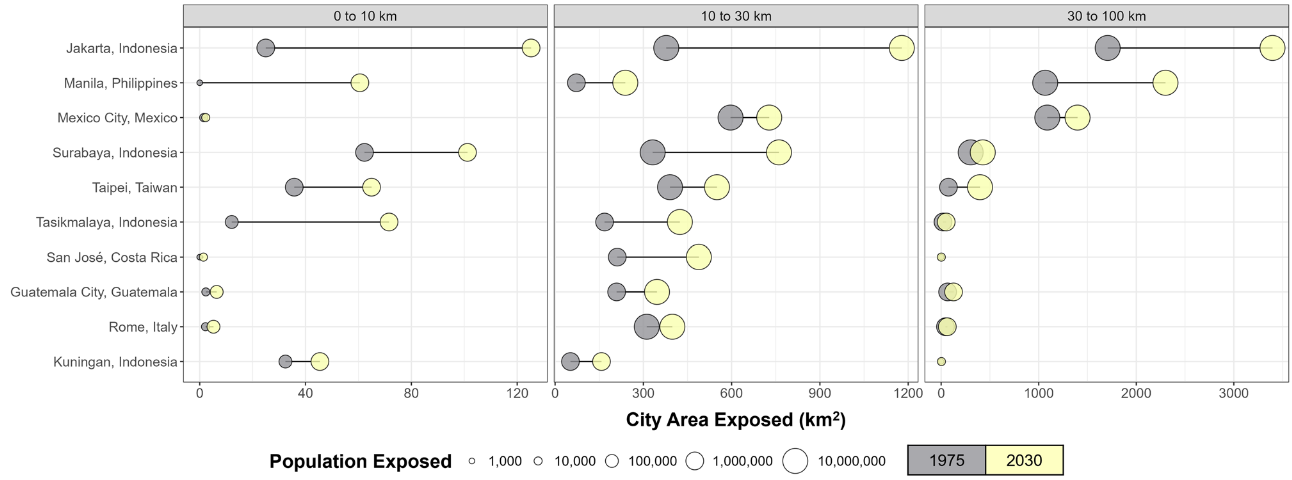

Fig. 6 | City area when the city was first exposed (grey) and city area in 2030 (yellow). City areas are within each buffer zone for the ten cities that span across all three distance buffers (0–10 km; 10–30 km; 30–100 km). The size of the points indicates the population exposed in the area within each buffer zone.

Prevailing winds suggest tephra from both Guagua Pichincha and Atacazo volcanoes may be directed away from the city under typical conditions. However, Quito and nearby Cumbaya are exposed to tephra fall from volcanoes to the east of the city (Fig. 9F). Flows from nearby volcanoes Guagua Pichincha and Atacazo are more likely directed away from the city (Fig. 9F). However, continued growth to the south of the city increases the proximity of populations towards the Atacazo volcano.

Manila, Philippines

Manila, the capital city of the Philippines, located within 100 km of four volcanoes, has one of the greatest rates of change in exposed area within 100 km from volcanoes, projected to reach over 30 million people in 2030, overtaking Tokyo (Fig. 8). Its population exposure has increased substantially over the past three decades into neighbouring provinces, particularly towards the north closer to Pinatubo, and to the south, closer to Taal (2025), San Pablo Volcanic Field (1350), and Banahaw. The city expanded by 60 km^2 into the 10 km buffer from 1975 to 2030 (Fig. 7), creating exposure within this buffer and placing residents closer to volcanic hazards (Fig. 9G).

Prevailing winds would likely carry tephra from Taal and Pinatubo (2021) towards the southwest, away from the city (Fig. 9G). Ongoing urban expansion increases the likelihood that larger populations may be affected by tephra fall. In the southeast of Manila, the expansion of smaller cities, including San Pablo, towards the Banahaw volcano coincides with areas in possible flow pathways (Fig. 9G).

Discussion

Our study extends previous global assessments by providing the first integrated spatio-temporal analysis of urban expansion and population change near Holocene volcanoes from 1975 to 2030, incorporating projections and directional growth metrics. Globally, the exposure of cities to potential volcanic hazards is increasing. From 1975 to 2030, the number of cities within 100 km of volcanoes increases by 106%, and the city population exposed rises by 154%. This trajectory is shifting exposure and likely impacts from rural to major urban areas. Globally, we find 52% of populations within 100 km of volcanoes will be living in cities by 2030 (Table 1). The rate of population growth within these city areas is higher than outside. These densely populated cities have expanded in size, and approximately half of those that are in more than one buffer distance are expanding towards volcanoes (Fig. 7). These trends show that urban growth is increasing population exposure near volcanoes, which may contribute to increasing volcanic risk and raise the likelihood that future volcanic eruptions will directly affect cities. This has also been found for other hazards, where urban areas will be disproportionately affected[55–57].

Most exposure increases occur in Southeast Asia, but there is also emerging growth in East Africa. Although population densities are increasing at all distances, density tends to rise faster at greater distances. In Mexico and Central America, both population and population density are higher at closer distances to volcanoes, although densities have largely plateaued since 2000. In Mexico and Central America, higher population numbers and density near volcanoes until the 1990s, shown in Figs. 3 and 4 likely reflect a history of establishing settlements in the highlands on fertile volcanic soils and in cooler climates[22,25,58,59], and the urban primacy of capital cities such as San Salvador and Guatemala City prior to 1990[60]. Cities occupy deposits of past large-scale eruptions, such as San Salvador and Naples, from past VEI 7 eruptions of Ilopango (429 CE) and Campi Flegrei (~39 ka), respectively[61–63]. In Southeast Asia, where city populations are also higher near volcanoes, population densities declined until around 1990 but have risen steadily since.

By contrast, in regions such as East Africa and North America, city populations are more spatially dispersed with higher populations away from volcanoes (Fig. 3), reflecting greater suitable land availability for city expansion[8], as well as fewer volcanoes than other regions[22]. The higher population number and density near volcanoes in Mexico and Central America compared to other regions (Fig. 3 and Fig. 4) are consistent with the findings of Gu[57] and Guimarães et al.[58], who ranked the region as having the highest population exposure to volcanic hazards and fourth globally when combined with hazard and vulnerability. The drivers behind these city patterns vary substantially between contexts and cannot be reliably inferred at a global scale. Some regional differences may also reflect the distribution of volcanoes and population centres.

The distribution of exposed populations around volcanoes also reflects geographic constraints. Global city populations cluster mostly within 20–30 km from volcanoes (Fig. 3), zones that can be reached by VEI > 5 eruptions. This corresponds with earlier studies on total populations, including outside of cities; Small and Naumann[22] found that population density decreased with distance from volcanoes, and Freire et al.[21] found a peak in exposure at 10–30 km from volcanoes. By focussing on cities rather than total population, our results highlight how urban populations are concentrated within distance bands and how these patterns change through urban expansion and densification over time. This advances on Meredith et al.[27], which identified most exposed cities for a single time period using a 2020 dataset, by examining how city populations and footprints change through time.

Topographic and natural constraints, including exclusion zones, appear to dictate the distribution and spread of city populations in these regions. For example, Naples, Jakarta, Tokyo, and Manila are situated along coastlines, while Quito and San Salvador have expanded along topographic

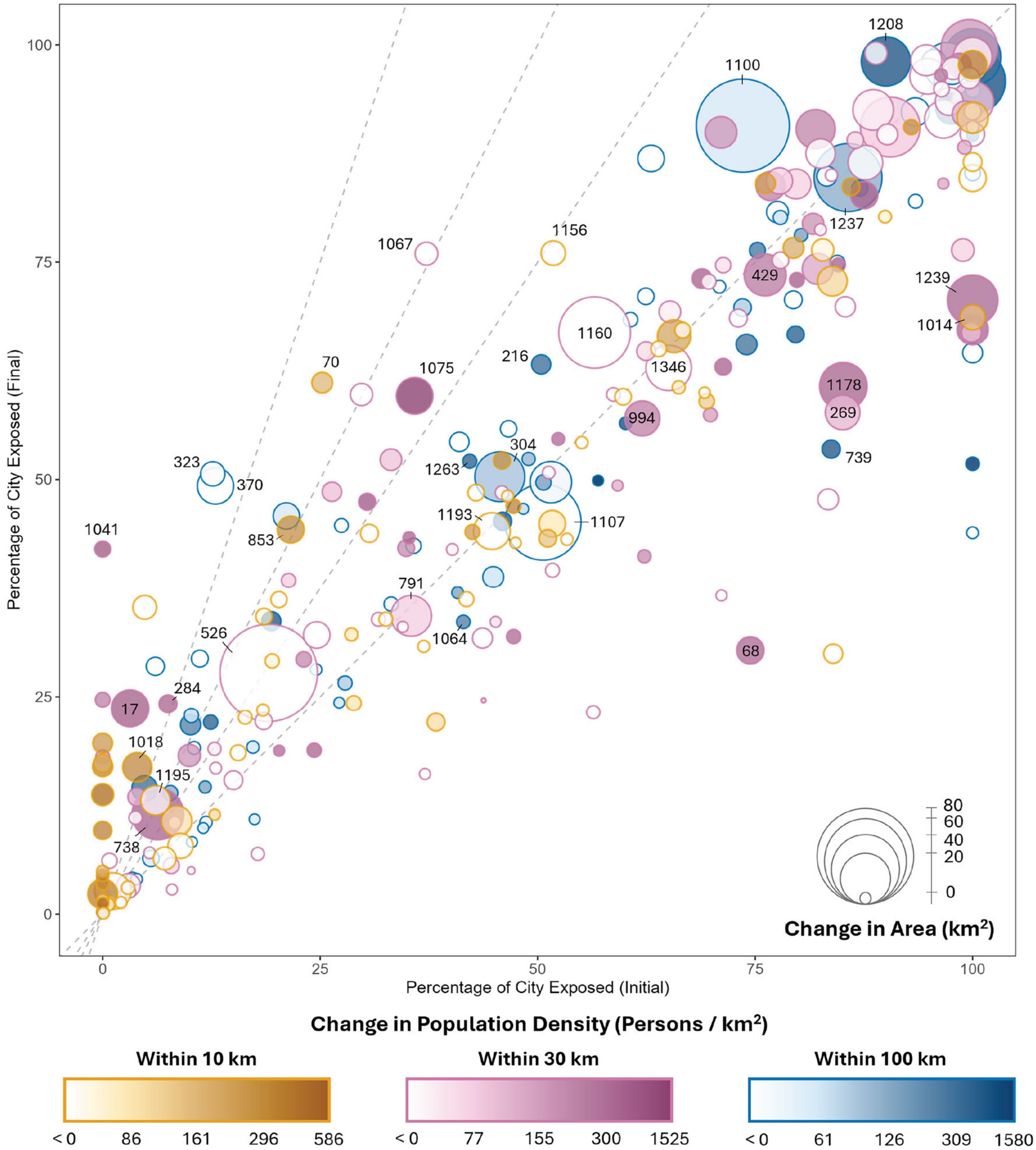

City ID	City	Country	City ID	City	Country	City ID	City	Country
17	Addis Ababa	Ethiopia	739	Manisa	Turkey	1156	Sumedang	Indonesia
68	Angeles	Philippines	791	Mexico City	Mexico	1160	Surabaya	Indonesia
70	Antigua Guatemala	Guatemala	853	Nakuru	Kenya	1178	Taipei	Taiwan
216	Butuan	Philippines	994	Puebla	Mexico	1193	Tarogong	Indonesia
269	Cilegon	Indonesia	1014	Quetzaltenango	Guatemala	1195	Tasikmalaya	Indonesia
284	Colima	Mexico	1018	Quito	Ecuador	1208	Tehran	Iran
304	Dagupan [Lingayen]	Philippines	1041	Rutshuru	DR Congo	1237	Tokyo	Japan
323	Denizli	Turkey	1064	San Jose	Philippines	1239	Toluca	Mexico
370	Eugene	United States	1067	San Juan Sacatepéquez	Guatemala	1263	Tuluá	Colombia
429	Guatemala City	Guatemala	1075	Sana'a	Yemen	1346	Yogyakarta	Indonesia
526	Jakarta	Indonesia	1100	Seattle	United States			
738	Manila	Philippines	1107	Seoul	South Korea			

Fig. 7 | Percentage of city area exposed in 2030 (Final, Y-axis) against percentage of city area exposed when the city was first within 100 km of a volcano (Initial, X-axis). The city area exposed refers to the city area within 10, 30, and/or 100 km of a volcano. The size of the circle represents the average rate of increase of area exposed for the city, in square kilometres per 5 years. The fill colour of the circle represents the average change in population density, in persons per square kilometre, for a 5-year period. White indicates a decrease in population density whilst increases in population density are shown on a percentile-based colour bar. The dotted lines indicate the relative rate of city growth in areas exposed compared to the total growth of the city e.g., gradient of line = 2 indicates that the relative increase in the area exposed is twice that of the increase in total city area. Key cities are labelled with the City ID and named with the country in the table below the graph.

corridors. Settlement locations around volcanoes are likely defined by natural constraints and the location of resources, as well as other factors such as governance. Populations generally settle at lower elevations[22] and constraints such as steep topography and exclusion zones may limit settlement closer to volcanoes, shown by the lower population number (Fig. 3) and densities (Fig. 4) within 10 km of volcanoes. For instance, in Japan, less than 1% of the city population lives within 10 km of a volcano, which could be a result of land-use planning efforts[64,65]. Volcanic hazard zonations have restricted certain land-uses in high-hazard areas, such as at Sakurajima[66], and elsewhere at Montserrat[67], Vesuvius[68], and in New Zealand[69]. The regions where there is high population density within 10 km of volcanoes are mostly in island nations where natural constraints restrict the available area for settlement, also highlighted in Meredith et al.[27]. However, city populations located less than 30 km from volcanoes are still within reach of VEI > 3 eruptions and impacts[48].

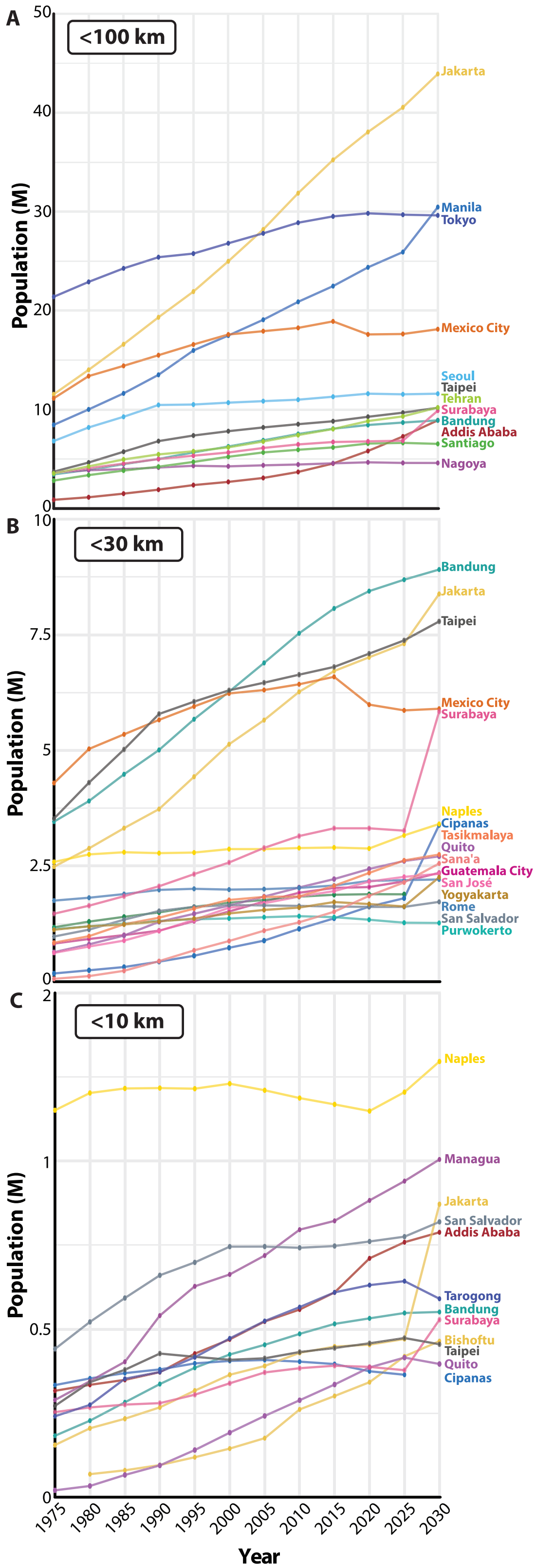

Fig. 8 | Most exposed cities through time. City population exposure for top cities is shown within **A**) 10 km, **B**) 30 km, and **C**) 100 km from Holocene volcanoes. Lines represent cities ranked among the top ten for at least one of the years for each distance. Note that the y-scale for each plot is different.

In addition to these spatial patterns, urbanisation processes influence how cities expand around volcanoes, which vary widely, reflecting topography, governance, and socio-economic drivers. Our results point towards exposure growth that is cumulative, episodic, uneven, and often preferential towards volcanic hazards. Around 85% of cities near volcanoes have expanded, and 59% densified their exposed area within at least one five-year interval. In general, larger cities expand and densify, while smaller cities often expand without major density increases. Natural constraints such as steep slopes or water bodies can limit expansion, while governance measures or transport links may influence expansion directions. Exposure and density thresholds could serve as indicators for prioritising land-use regulation, helping to steer development away from high-hazard zones before they densify. In general, the finding that around half of the cities that span across multiple buffers are expanding towards the volcano highlights how directional growth increases exposure to a wider range of volcanic hazards and eruption sizes, as cities moving closer to the volcano face more proximal hazards (e.g., lava flows, pyroclastic density currents, ballistic projectiles), as well as larger explosive eruptions.

At regional and local scales, the exposure metrics highlight spatial patterns that can help contextualise local development dynamics. The growth of cities, particularly in Southeast Asia and East Africa, reflects recent decades of rapid urbanisation and infrastructure expansion[70,71]. Within cities, population growth may cause urban saturation, leading to housing affordability pressures and investments into infrastructure away from the city centre, pushing development outward, converting land to urban areas[72,73,74]. There may also be the development of smaller nearby satellite cities and peri-urban areas. These are transitional zones located in the outskirts of a city[75], which were explored by Winarso et al.[76] to be occurring around Jakarta since the 1990s due to reasons such as an increase in migrants and household income, perhaps reflected by the growing smaller cities around Jakarta in Fig. 9. Merging of these smaller cities with Jakarta likely led to the rapid increase in exposure to volcanoes shown in Fig. 8. However, regionally, in Southeast Asia, a decline in densities near volcanoes until the 1990s (Fig. 4) may correspond to more coastal urbanisation and industrialisation[77] that drew populations away from upland volcanic areas. This trend is also seen in Mexico and Central America, where population densities near volcanoes plateau after 2000. This may reflect broader regional patterns, including the growth of lowland cities[78], the expansion of secondary and peri-urban cities around national capitals[79,80], increased international emigration[81], increasing appreciation of volcanic threats[82,83].

Localised drivers influence how and where cities expand around volcanoes, often pushing growth into more hazardous areas and often occurring more in marginalised and poorly regulated settlements due to affordability and governance gaps[84,85]. In San Salvador, rapid and unregulated expansion since the 1970s has led to settlements on the slopes and ravines on San Salvador volcano, due to land scarcity and scenic preferences[86–88], highlighted by the steep increase in population <10 km of volcanoes between 1975 and 2000 in Fig. 8. Cities may also be expanding towards volcanoes due to investments in tourism infrastructure closer to volcanoes[89]. Examples include the growth of Tagaytay overlooking Taal volcano (Fig. 9G) or Legazpi City on the slopes of Mayon in the Philippines, as well as the development of Rotorua in New Zealand, which have been tied to tourism (Erfurt-Cooper, 2014).

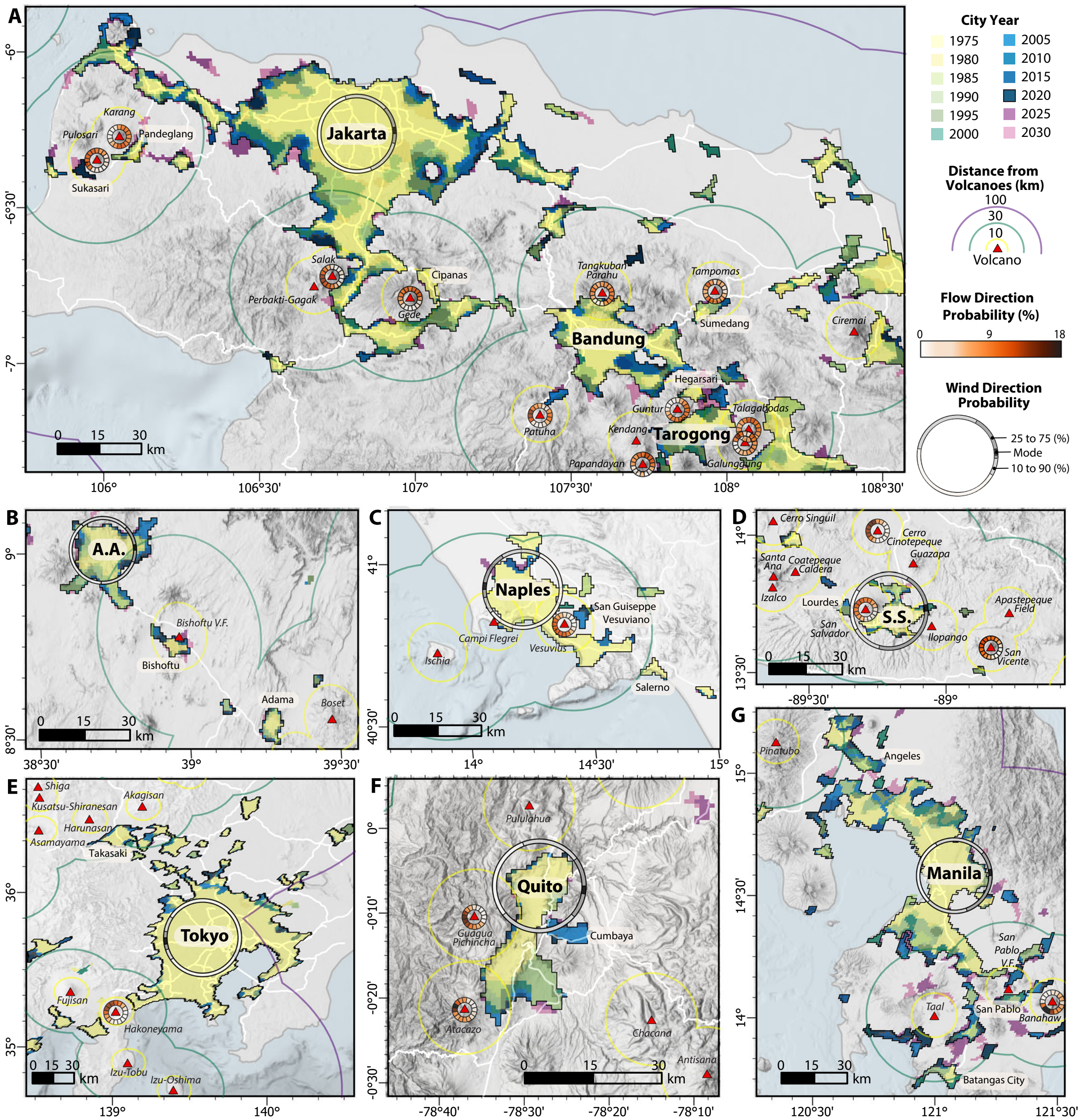

Fig. 9 | Case study areas of spreading cities. Maps show city polygons for **A**) Jakarta, Bandung, and Tarogong, Indonesia, in Southeast Asia, **B**) Addis Ababa (A.A.) Ethiopia, in East Africa, **C**) Naples, Italy, in Europe, **D**) San Salvador (S.S.), El Salvador, in Central America, **E**) Tokyo, Japan, in East Asia, **F**) Quito, Ecuador, in South America, and **G**) Manila, Philippines, in Southeast Asia. Other key cities are also highlighted. Colours of polygons show the past and projected locations of the city through time. Rings around volcanoes show FlowDIR-derived directional likelihoods for topographically controlled hazardous flows (lava flows and dome-collapse derived block-and-ash flows), normalised to sum to 100%, with values ranging from lower (white) to higher (brown). Rings around bold city names show predominant wind direction over the city, with black as the most common direction (i.e., the direction that the wind is blowing from). Wind and flow directions are illustrative indicators of potential hazard pathways and do not represent eruption-specific hazard footprints. Volcano names are given in italics. Key highways from OpenStreetMap[133] are shown in white, waterbodies are from Natural Earth[134], and 30-m DEMs are from Copernicus[135]. V.F. refers to a volcanic field.

These expansions into hazard zones are occurring despite hazard awareness. The increasing exposure of cities close to volcanoes suggests that, where effective monitoring and DRR frameworks are in place, continued settlement in monitored hazard zones may be perceived as acceptable or low-risk[90,91]. Since the 1990s, many developing regions have established or strengthened volcano observatories and early warning systems[92], helped by global initiatives such as the UN International Decade for Natural Disaster Reduction (1990 to 2000)[93], which may give a sense of security to those living close to volcanoes[94]. Research also shows that people in rural areas have a higher perceived risk than in cities[95,96], suggesting urbanisation creates a sense of distance of the urban population from the volcano. This is also seen for other hazards[35]. The benefits of living in a city may outweigh the potential risks of eruptions.

Land scarcity and constraints may also limit growth in some areas, pushing populations into higher-hazard areas. Some cities, such as Surabaya and Tasikmalaya in Indonesia, and San Jose in Costa Rica, see limited growth further away from volcanoes (Fig. 6), likely due to topographic constraints that control the shape and orientation of the cities as they expand. Steep topography to the east and west of the city is limiting the expansion of Quito to north-south directions[97] (Fig. 9F). Major coastal cities such as Manila, Jakarta, and Naples are located between volcanic slopes and the sea (Fig. 9), concentrating dense populations within 20–60 km of volcanoes, and expanding along the coastlines.

City growth is not uniform; many cities are expanding more rapidly towards hazardous areas than other parts of the city and other cities (Fig. 7). Most cities have expanded more than once, suggesting that while exposure growth is long-term and sustained, the drivers may be tied to specific events or phases such as infrastructure development or post-disaster rebuilding (Fig. 5). Examples include the highway-driven expansion between Jakarta and Bandung, the governance-driven growth of Naples, or the population growth of Addis Ababa and Manila driven by their political and economic role[74,98,99]. Broader urban change studies show that exposure and impacts are coupled through development[20,100]. Long quiescent periods of volcanic activity encourage settlement (e.g., Vesuvius after 1944[101]), whilst eruptions may temporarily reduce exposure (e.g., reduction in population around Unzen after 1991[102]) or be followed by rapid rebuilding (e.g., Goma after the 2002 Nyiragongo lava flows[103]). Some of the episodic changes we observe may also reflect the structure of the GHS-POP dataset itself, with census data collected at intervals. However, identifying key moments of exposure increase and the triggers would be important for intervention and mitigation strategies.

This also means that the potential for cascading impacts affecting national through international scales increases, particularly as cities become interconnected and merge together. The *city polygons* used in this study, defined by high population density, represent areas where there are dense concentrations of buildings and infrastructure. As seen during past eruptions, such as at Nyiragongo 2002 and Pinatubo 1991, our dependence on critical infrastructure[37] and the role of cities as economic and political hubs[36], mean that the effects of volcanic eruptions on a city will likely be severe and cascade beyond the direct impact area[27,104].

The increasing growth in city exposure and interconnectedness of cities suggests that future eruptions will have cascading effects beyond the direct impact zone. This merging is shown between 2025 and 2030, for example, by the jump in exposure 10 km from volcanoes for Jakarta, and 30 km from volcanoes for Surabaya (Fig. 8). The highly exposed cities of Jakarta and Bandung have expanded toward each other following the major highway that connects them along the Jakarta-Bandung mega urban corridor[105,106], reducing their separation from 25 km in 1975 to a projected 16 km by 2030. Such infrastructure networks may propagate impacts between cities as they become more interconnected, increasing the potential for widespread regional disruption.

Despite the merging of cities through time, a single eruption is likely to affect multiple cities at once as the absolute number of exposed cities is increasing[27] (Fig. 2). This has been exemplified in past events where multiple settlements have been affected by a single eruption. For instance, tephra from the 2018 Fuego eruption affected Guatemala City and Antigua, affecting transport and evacuation routes[107] and the 2011 Cordón Caulle eruption saw impacts to multiple cities, including San Carlos de Bariloche and Neuquén, while tephra fall caused flight cancellations in Buenos Aires[108]. The trends in increasing number, merging, and interconnectedness of cities shift risk from a local to a regional scale, bringing competing demands for resources and challenges in evacuation and recovery planning.

These dynamics can be further illustrated through local examples given in this study. In some cities, such as Jakarta and Bandung, our directional exposure metrics capture expansion along major transport corridors and into specific hazard-prone sectors. Key examples show cities spreading preferentially towards volcanoes and sometimes towards likely flow paths or wind directions (Fig. 7). The rate of growth in exposed areas relative to the total city growth was higher for almost half of the cities spanning across multiple buffer zones. In land-constrained contexts, complete avoidance of volcanic hazard zones may be unrealistic; therefore, proactive, risk-informed mitigation efforts and planning is important to reduce future effects of eruptions. Our research identifies key city hotspots where localised risk assessments and targeted mitigation efforts should be prioritised.

The global scale assessment allows for the identification of key trends of expansion towards volcanoes, but understanding whether directional city growth aligns with likely hazard pathways is essential to assess volcanic exposure on a local scale. Integrating exposure trajectories with hazard pathways, such as those shown in Fig. 9, would support development and risk-reduction planning. Several cities we examined lie directly in the direction of possible flow paths, such as Naples and San Salvador, and, in some cases, city spreading has expanded towards possible flow pathways, such as in Taragong and Sumedang in Indonesia (Fig. 9). We highlight where future expansion may intersect possible flow pathways, including the growing connection between Tarogong and Hegarsari near Guntur, expansions of Cipanas and Jakarta towards Gede, and San Pablo towards Banahaw. These cases show that relating city expansion to hazard pathways is crucial to identify key areas of high or escalating exposure.

Mapping these local patterns allows hazard managers to identify growth corridors for intervention, perhaps where city density or area reaches a certain threshold, to require stronger codes; our metrics can act as those thresholds. These patterns can also guide the spatial prioritisation of monitoring, preparedness, and evacuation planning by highlighting sectors of the city where exposure is increasing more rapidly. For land-constrained nations and cities, densification plans and hazard adaptations may be more suitable than restricting outward growth. As cities become more interconnected, these metrics also help identify where co-ordination between cities is needed, particularly where multiple cities are expanding towards volcanoes.

Other local examples show possible flow directions and predominant winds oriented away from key cities, yet they are exposed to other hazards or from more distant sources, and local winds can produce varying exposure patterns. For example, possible flow directions from Guagua Pichincha and Atacazo are away from Quito. Lahars from Cotopaxi farther away reached the southeastern outskirts of the city[109,110], where urban expansion is occurring (Fig. 9). Around Tokyo, flow paths from Hakoneyama are oriented away from the city, yet surrounding populations occupy areas inundated by Fujisan lahars ~22 ka[111] (Fig. 9E), and the city has been affected by tephra from distant volcanoes Sakurajima (1914; ~950 km) and Asama (1983, 2004; ~140 km)[112,113]. Similar examples have occurred in the past with tephra fall impacts in San Salvador[53,52]. Addis Ababa, while unlikely to be affected by flows from nearby vents[114], geological evidence indicates potential future activity from volcanoes farther away, such as Furi and Wonchi[74]. In Indonesia, consistent with our predominant wind directions towards the west, tephra fall has reached Bandung from Galunggung in 1982 (ref. 115), and with predominant winds to the east, Tokyo has been affected by tephra fall from Fujisan, such as in 1707[116]. However, despite our typical wind patterns suggesting limited exposure, tephra fall from Guagua Pichincha affected Quito in 1999, Naples was impacted by Vesuvius in 1944[117], Jakarta from Gede in 1948[118], and Manila from both Taal in 2020 and Pinatubo in 1991[33,119]. These examples demonstrate that although our results provide key insights, local-scale exposure carries inherent uncertainties due to factors such as variable wind patterns, which limit local-scale interpretation of the results.

The trend of cities spreading into high-hazard areas is also found when looking at exposure to other hazards. For instance, there are increases in populations in floodplains[3] and seismic zones[14]. Volcanic exposure may overlap with other high-hazard areas, amplifying risks. Secondary hazards, including the remobilisation of volcanic deposits, may also occur due to triggers such as rainfall or earthquakes. Jakarta, for instance, combines volcanic exposure with flooding, earthquakes, and subsidence[26], while Addis Ababa faces combined hazards from volcanoes and ground-water driven subsidence[120]. Such compound hazards complicate planning because impacts are amplified and difficult to forecast. Land-use planning should also consider exposure to other hazards.

Several limitations should be considered when interpreting these results. We quantify global exposure using distance metrics, and the selected case studies are illustrative examples used to contextualise exposure trends, rather than conducting a local hazard assessment. Distance buffers provide a practical and globally consistent approximation of potential exposure, enabling comparison across volcanoes in the absence of standardised hazard footprints. Exposure estimates derived from these distance buffers may locally overestimate or underestimate exposure, as explored in Biass et al.[48]. However, our analysis identifies broad trends in spatio-temporal exposure. Population estimates for 2025 and 2030 are projections from GHS-POP[121] and therefore have uncertainty associated with demographic forecasts and downscaling assumptions.

We used the GVP database for the location of Holocene volcanoes, including volcanic fields, which introduces uncertainty because the vent location of future eruptions is unknown[27]. Exposure estimates are likely to slightly vary depending on the version of the GVP database of Holocene volcanoes used, as updates refine locations of vents or update the list of volcanoes active in the Holocene. However, these would likely not alter the broader exposure patterns found in this study. Volcanic systems are heterogeneous in eruption frequency and eruptive style. For Fig. 9, our flow-direction analysis represents topography-based estimates of potential flow directions and does not quantify the likelihood of different eruption styles or the occurrence of specific flow hazards, which requires more localised analysis. Flow-direction analysis was also not conducted for volcanic fields. For areas potentially exposed to tephra fall we only considered prevailing winds, yet seasonal wind variations influence tephra dispersal and exposure patterns. The metrics and illustrative indicators here do not imply uniform behaviour or eruption likelihood, and do not replace local hazard and risk assessments. The results provide an indication of where urban populations are concentrating in relation to volcanoes.

In this study, we provide a foundation for assessing city expansion near volcanoes on a global scale. Future work can build on this framework by incorporating more detailed hazard and exposure data to refine and localise assessments. Future global assessment could incorporate a classification of volcanoes by recent activity or a hazard index. For more detailed hazard analysis at individual volcanoes, spatio-temporal exposure can be compared with local hazard maps. For exposure data, we used a population density of >1500/km^2 to define city areas, which does not include peri-urban and rural populations or agriculture, which have different exposures and vulnerabilities. The *city polygons* present areas of highly dense building and infrastructure, a detailed assessment using data regarding specific building and infrastructure types can help to identify key vulnerabilities more accurately. Disaggregating exposure data by population or building types could improve understanding of these social and spatial patterns, while future research could also examine how different land-use trajectories influence exposure to volcanic hazards. As higher-resolution Shared Socioeconomic Pathway (SSP) population exposure datasets become available, these could be used to extend exposure projections beyond 2030, enabling more detailed exploration of future exposures around volcanoes. Expanding this framework to include temporally variable wind patterns and hazard footprints would improve the exposure estimates.

Beyond proximity-based measures, future analyses could also incorporate weighted exposure indices that reflect a broader range of physical or social conditions. For example, these might include metrics derived from past eruption impacts (e.g., affected areas, or PEI using historical fatality distances), socio-economic indicators such as the HDI, or inequality indices such as GINI. Physical and environmental factors such as slope, climate-related stressors, or water bodies could also be integrated to capture how local geography shapes exposure. In addition, considering the proximity and connectivity between neighbouring cities and infrastructure could help capture cascading impacts, as disruptions in one city may amplify impacts in others nearby.

With our local case studies, we explore some example drivers of urban exposure change. However, there could be further analysis of the reasons for exposure changes around volcanoes. Factors such as migration, demographic changes, and risk perception may influence future exposure patterns. With higher temporal-resolution exposure data, it may be possible to explore the effect of eruptions themselves on exposure changes. For example, it has been noted that there was an increase in populations around Vesuvius, Italy, due to the quiescence after the 1944 CE eruption[101], while there was a decrease in younger populations in cities near Unzen volcano, Japan, due to fear and the destruction caused, after the 1991 CE eruption[102]. Our study goes to 2030, and does not extend further in time as the exposure datasets beyond these years have lower resolutions. However, longer-term exposure incorporating alternative socio-economic pathways, depending on urban policy, migration, and climate-driven relocation, could refine future assessments.

Methods

We developed a framework to assess spatio-temporal trends in city population exposure to volcanic hazards (Fig. 10). The approach for compiling a dataset of exposed cities and their populations is based on the methodology used in Meredith et al.[27] but applied across multiple years. Below, we present how we prepared the multi-year city exposure population dataset, generated spatio-temporal metrics, and analysed the change in global and local city population exposure over time and distance from volcanoes. We refer to *exposed populations* as populations within cities and less than 100 km from at least one volcano active in the Holocene. The R code used to generate the results is provided: https://github.com/vharg/VolcCities-Temporal. We used the web app generated in Meredith et al.[27] to present the results of this study, showing the city outlines through time for cities with over 100,000 people in 2020. The app is available here: https://vharg.github.io/shiny_VolcCities/.

Datasets used

To explore changes in city exposure to volcanic hazards over time, we generated 12 datasets of cities and their populations within 100 km of volcanoes active in the Holocene, one for each 5-year interval between 1975 and 2030. The spatial representation of these cities will be referred to as *city polygons*.

The *city polygons* used in this study were derived from the Global Human Settlement Layer – Urban Centres Database (GHS-UCDB R2023A) dataset of global *urban centre* geometries, projected in Mollweide coordinate system at 1 km x 1 km resolution[122]. For each timestep (5-year intervals), the GHS-UCDB dataset identifies *urban centres* as having a total population size of at least 50,000 people and having a population density of ≥1500 inhabitants per square kilometre. The datasets for 1975 to 2020 are based on observed population and built-up surface data, while the 2025 and 2030 datasets rely on projected population and built-up surface area estimates[122]. City names for the 2025 dataset were taken from the GHS-UCDB (R2023A) point dataset of urban centres and, if missing, were supplemented from the GHS Degree of Urbanisation Classification (GHS-DUC R2023A) dataset[123]. Country names and regional classifications were based on the Natural Earth "Admin 0 – Countries" (1:10 m cultural vectors) dataset that provides country boundaries[124].

Population data were taken from the Global Human Settlement Population (GHS-POP R2023A) data, which provides gridded estimates at 1 km x 1 km spatial resolution for the time periods between 1975 and 2030, projected in the Mollweide coordinate system[121]. Unlike LandScan, which estimates ambient population (i.e., including commuters and tourists, etc.), GHS-POP estimates resident population by spatially distributing census counts over grid cells based on the location of built-up areas extracted from satellite imagery[125]

Locations for 1264 volcanoes were taken from the Global Volcanism Program[126] dataset of volcanoes active in the Holocene, which we refer to as Holocene volcanoes (version 5.2.7), which also provides information on volcano type and eruptive history. All volcanoes within the dataset were included. Coordinates of the Holocene volcanoes in the database are positioned either at the summit for volcanoes with a distinct primary edifice or close to known vents. For volcanic fields with multiple vents, the database

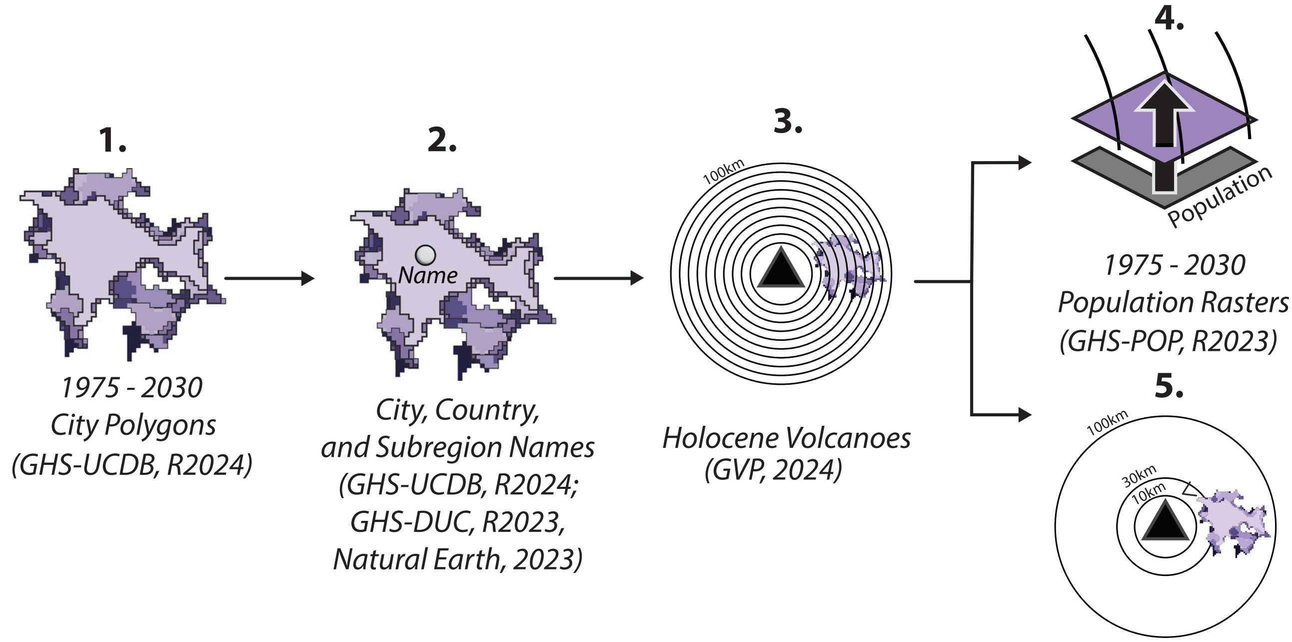

Fig. 10 | Schematic illustrating the methodology used to assess changes in city exposure to volcanic hazards over time. 1) City polygons were taken from GHS multi-temporal settlement datasets (1975–2030: GHS-UCDB MTUC); **2**) City polygons were attributed with 2025 city, country, and subregion names from the GHS-UCDB point, GHS-DUC polygon, and Natural Earth polygon datasets. **3**) Concentric buffer zones were made (10–100 km at 10-km intervals) around Holocene volcano locations (GVP, 2024); **4**) Population within each buffer zone was extracted from GHS-POP rasters (1975–2030: GHS-POP R2023) to assess global and regional spatio-temporal trends in population exposure; **5**) Buffer zones were aggregated into 10-, 30-, and 100-km distance bands, and city polygon areas were calculated within these bands to derive city exposure metrics quantifying how exposure shifts toward or away from volcanoes over time.

presents the most prominent or active vent, the most recently erupting vent, or the centre of the entire volcanic field, depending on information availability. Using a single point to represent distributed volcanism introduces uncertainty, as the precise location of future eruptions is unknown.

Compiling the Global Exposed City Dataset

We created 100 km buffers around the 1264 Holocene volcanoes from the Global Volcanism Program[126] database. For each year, between 1975 and 2030, in 5-year intervals, we selected *city polygons* fully or partially within these 100 km buffers. Following the minimum resolution of the underlying GHS-UCDB dataset, city polygons with an area of less than 1 km^2 within 100 km of a volcano were excluded. This removed 28 city polygons across 7 cities between 1975 and 2030, as well as 14 other cities completely from the dataset.

For the *city polygons* attribute data, city names for 2025 were assigned by spatially joining each city polygon with the corresponding point in the GHS-UCDB MTUC city points dataset[122], ensuring that each polygon was matched to a single point. The city polygons were then spatially joined with Natural Earth[124] country boundaries, and country names and subregions were assigned based on the largest overlap, or nearest country if there was no overlap present. These regional classifications are based on UN Geoschemes. *City polygons* were merged where both the city name and country name matched, aggregating spatially fragmented urban areas into unified cities. This resulted in a total of 1173 unique *city polygons* for 2025, where each row of the attribute table corresponds to one city. To ensure consistent naming, each city polygon was assigned the name of the polygon in the adjacent time step with which it had the largest spatial overlap (propagating backward from 2025 to earlier years and forward from 2025 to 2030). Polygons that remained unnamed after this step (e.g., they were not in the 2025 dataset) were assigned names by joining them to the closest matching polygon from the GHS-Degree of Urbanization Classification dataset, based on the Name_2 column. This iterative approach ensured consistent naming across time while filling gaps.

Different cities may share the same name, for example, there are two cities named San Carlos in the Philippines, one in Pangasinan (North) and the other in Negros Occidental (Central). Therefore, all cities, based on their spatial location between 1975 and 2030, were assigned a city ID number in alphabetical order so that, for example, the two San Carlos' in the Philippines had different city IDs. Every city polygon from each year was tagged with its city ID to track the growth of the city through time.

We extracted population data for each city polygon from the corresponding year of the GHS-POP R2023A rasters[121], calculating population exposure at ten distance intervals from each volcano. This included both cumulative buffers (e.g., within 10 km, 20 km, up to 100 km) and ring buffers representing distinct zones (e.g., 10–20 km, 20–30 km, etc.), each spaced at 10-km increments. For cities partially within 100 km of a volcano, only the population within 100 km was counted. For the global analysis, we used all ten 10-km ring buffers, and for city-level analysis, we used 10-km, 30-km, and 100-km cumulative buffer counts, as these distances correspond to average maximum distances of primary life-threatening volcanic hazards[47,48].

In total, we produced 12 globally exposed city population polygon datasets, covering the period of 55 years and spanning 582 cities in 1975 to 1196 cities in 2030. Across the study period, 773 new cities were added since 1975, and 162 cities that were no longer within 100 km of a volcano were removed from the dataset. These datasets are provided in Supplementary Data 1 for population exposure per year, and as growth metrics in Supplementary Data 2. For Supplementary Data 1, each sheet corresponds to each year. The temporal distribution of when volcanoes first become associated with cities is shown in Supplementary Fig. 1. A web application was also developed to visualise these results interactively, accessible at: https://vharg.github.io/shiny_VolcCities/.

Spatio-temporal metrics

To assess city expansion towards or away from volcanoes, we generated a dataset measuring the distance between city polygons and nearest Holocene volcanoes located within 100 km for each year, which is presented in Supplementary Data 2. For global and regional assessment, we calculated the total city area (km^2) within each 10-km ring buffer, and the city population density within the ring buffers using Eq. (1):

$$PD_{b,t} = \frac{Pop_{b,t}}{Area_{b,t}} \quad (1)$$

where PD_b is the averaged city population density within buffer *b*, Pop_b is the total city population within buffer *b*, and $Area_b$ is the city area (km^2) within buffer *b*, each for the corresponding year *t*. This was used to analyse population and population density distribution around volcanoes through time. At the city level, population density was calculated similarly, but using the cumulative buffers at 10, 30, and 100 km.

On a city level, to evaluate change in city exposure, we selected projected cities from the 2030 dataset that were also exposed in at least one time period prior to 2030, and calculated two core growth metrics. We aggregated temporal and spatial exposure to analyse changes within 10-, 30-, and 100 km interval distances from volcanoes. Urban expansion is commonly quantified as the rate of change per unit time, such as the urban spatial expansion index[127] and urban expansion speed[128]. Building on these concepts, we calculated the absolute rate of change for both the urban area exposed and the average population density in these areas. The absolute rate of change quantifies the average rate of growth in 5-year periods and is defined using Eq. 2:

$$\text{Absolute rate of change} = \frac{Final\ value - Initial\ value}{N_{years}} \quad (2)$$

where Final value and Initial value refer to either the exposed urban area (km^2) or exposed averaged population density (people/km^2) depending on the rate of change being calculated, and N_{years} is the number of 5-year time intervals between the initial and final time step. This metric captures how rapidly exposure increases over time.

We also introduced a frequency metric (Eq. 3) to measure how often the city area expanded over the period it was exposed. This is represented as a percentage, where N_{inc} is the number of 5-year periods where the exposed city area increases, over the total number of 5-year periods (N_{years}).

$$Freq(\%) = \frac{N_{inc}}{N_{years}} * 100 \quad (3)$$

For cities spanning across multiple buffer zones e.g., within versus beyond 100 km, we also calculated the proportion of the city area in each zone when it was first exposed and in 2030 (projected). This metric is compared and used to identify preferential growth in buffer zones for each city. All formulas and metrics obtained for each city are provided in Supplementary Data 2.

Case studies

At a local level, we investigated spatio-temporal trends in city expansion near Holocene volcanoes for nine cities to discuss different potential drivers and patterns of growth for cities. The cities selected are Jakarta, Bandung, Tarogong (Indonesia), Addis Ababa (Ethiopia), Naples (Italy), San Salvador (El Salvador), Tokyo (Japan), Quito (Ecuador), and Manila (Philippines), which were selected from cities that are highly populated and highly ranked across the various metrics in different geographical regions. We mapped the city polygons over time to observe expansion patterns relative to nearby volcanoes. Additionally, we examined the relationship between urban growth and potential exposure to tephra fall from local volcanoes using the prevailing wind direction as tephra typically spreads and deposits in downwind areas[129]. The prevailing wind direction over the city centroid is represented by the 10-degree azimuth bin with the highest frequency for winds between 5 and 15 km above sea level over a 10-year period, extracted from the ECMWF ERA-5 dataset for 2015 to 2024[130]. Variability in wind direction is indicated by the 10th, 25th, 75th, and 90th percentile wind directions calculated across the same altitude range and years. We focused on the wind direction at an altitude of 5 to 15 km corresponding to the plume heights of smaller magnitude eruptions (up to VEI 4[131]) since these eruptions are more common and likely to deposit tephra within 100 km of the volcano. Supplementary Fig. 1 summarises prevailing wind directions across other altitude bands. For larger magnitude eruptions, where tephra may disperse beyond proximal regions, ash transport is governed by broader atmospheric circulation, rather than local wind conditions[130]. Prevailing wind directions represent long-term averages and do not capture seasonal variabilities.

To evaluate potential volcanic flow hazards, we applied the topography-based FlowDIR tool from Tennant et al.[132] to calculate probable flow directions. This is a first-order topographic approximation that does not replace detailed hazard assessments. Rather than simulating flow footprints, the method analyses a digital elevation model (DEM) of the volcano's summit to derive the directional likelihood distribution of travel directions within and away from the summit area for topography-controlled volcanic flows (lava flows and dome collapse-derived block-and-ash flows). The tool outputs normalised directional likelihoods derived from summit topography. For each of our case study cities, we selected Holocene volcanoes within 30 km of the city polygon for the year with the largest *city polygon* area. Thirty kilometres was chosen as a credible maximum distance for block-and-ash flows, with a 5% probability of exceedance[46]. To ensure accuracy in the flow direction assessment, we only considered volcanoes with a clearly defined summit (i.e., highly eroded volcanoes were excluded). We also excluded volcanic fields due to uncertainty in the location of the next eruption. A total of 19 volcanoes that fit the above criteria were selected for FlowDIR analysis. More information on volcano selection and data used is provided in Supplementary Data 4.

Data availability

The city exposure datasets generated in this study are available as Supplementary Data 1–3. The web application to visualise the results is available here: https://vharg.github.io/shiny_VolcCities/.

Code availability

The R code used to generate the results in this study is available at: https://github.com/vharg/VolcCities-Temporal.

Received: 9 December 2025; Accepted: 23 March 2026;
Published online: 09 April 2026

References

1. United Nations, D. of E. and S. A. (UN D. World Urbanization Prospects: The 2018 Revision. (New York: United Nations 2019).
2. Fekete, A. Peri-urban growth into natural hazard-prone areas: mapping exposure transformation of the built environment in Nairobi and Nyeri. *Kenya, from 1948 to today. Nat. Hazards* **119**, 859–882 (2023).
3. Rentschler, J. et al. Global evidence of rapid urban growth in flood zones since 1985. *Nature* **622**, 87–92 (2023).
4. Mitchell, J. K. Megacities and natural disasters: a comparative analysis. *GeoJournal* **49**, 137–142 (1999).
5. Rogers, J. S., Maneta, M. M., Sain, S. R., Madaus, L. E. & Hacker, J. P. The role of climate and population change in global flood exposure and vulnerability. *Nat. Commun.* **16**, 517 (2025).
6. Intergovernmental Panel on Climate Change (IPCC). Summary for Policymakers. in Climate Change 2022 – Impacts, Adaptation and Vulnerability 3–34 (Cambridge University Press, 2023). https://doi.org/10.1017/9781009325844.001.
7. Bangalore, M., Smith, A. & Veldkamp, T. Exposure to Floods, Climate Change, And Poverty in Vietnam. Econ. Disaster. *Clim. Chang.* **3**, 79–99 (2019).
8. Güneralp, B., Güneralp, I. & Liu, Y. Changing global patterns of urban exposure to flood and drought hazards. *Glob. Environ. Change* **31**, 217–225 (2015).

9. Tellman, B. et al. Satellite imaging reveals increased proportion of population exposed to floods. *Nature* **596**, 80–86 (2021).
10. Li, L. et al. Increasing population exposed to both seismicity and flooding in low-income countries. Geomat. Nat. *Hazards Risk* **16**, 2493217 (2025).
11. Ozturk, U. et al. How climate change and unplanned urban sprawl bring more landslides. *Nature* **608**, 262–265 (2022).
12. Rimal, B., Zhang, L., Keshtkar, H., Sun, X. & Rijal, S. Quantifying the spatiotemporal pattern of urban expansion and hazard and risk area identification in the Kaski District of Nepal. *Land* **7**, 37 (2018).
13. Ferrer, J. V. et al. Exposure to large landslides in cities outpaces urban growth. *Geophys. Res. Lett.* **52**, e2025GL115170 (2025).
14. Huang, Q., Meng, S., He, C., Dou, Y. & Zhang, Q. Rapid Urban Land Expansion in Earthquake-Prone Areas of China. *Int. J. Disaster Risk Sci.* **10**, 43–56 (2019).
15. Wang, H. et al. Rapid Growth of Population, GDP, and Built-up Land Exposed to High Seismic Hazard in Large Cities, China. Preprint at https://doi.org/10.20944/preprints202406.0705.v1 (2024).
16. Mohuya, F. A., Walsh, C. L. & Fowler, H. J. Urban flood risk management through the lens of citizen science: A case study on the two city corporations' area of Dhaka. *Int. J. Disaster Risk Reduct.* **124**, 105405 (2025).
17. Muis, S., Güneralp, B., Jongman, B., Aerts, J. C. J. H. & Ward, P. J. Flood risk and adaptation strategies under climate change and urban expansion: A probabilistic analysis using global data. *Sci. Total Environ.* **538**, 445–457 (2015).
18. Asian Development Bank. Building resilience of the urban poor: Recommendations for systemic change. (Asian Development Bank, 2022).
19. Godschalk, D. R. Urban Hazard Mitigation: Creating Resilient Cities. (2003) https://doi.org/10.1061/ASCE1527-698820034:3136.
20. Stolte, T. R. et al. VulneraCity–drivers and dynamics of urban vulnerability based on a global systematic literature review. *Int. J. Disaster Risk Reduct.* **108**, 104535 (2024).
21. Freire, S., Florczyk, A. J., Pesaresi, M. & Sliuzas, R. An improved global analysis of population distribution in proximity to active volcanoes, 1975–2015. *ISPRS Int. J. Geo-Inf.* **8**, 341 (2019).
22. Small, C. & Naumann, T. The Global Distribution of Human Population and Recent Volcanism. Environmental Hazards vol. 3 http://www.LDEO.columbia.edu/Bsmall/PopVol.html (2001).
23. Blaikie, P., Cannon, T., Davis, I. & Wisner, B. At risk: natural hazards, people's vulnerability and disasters. (Routledge, 2014).
24. Heiken, G. Dangerous Neighbors: Volcanoes and Cities. (Cambridge University Press, 2003).
25. Chester, D. K., Degg, M., Duncan, A. M. & Guest, J. E. The increasing exposure of cities to the effects of volcanic eruptions: A global survey. Environ. *Hazards* **2**, 89–103 (2000).
26. Pelling, M. The vulnerability of cities: natural disasters and social resilience. (Routledge, 2012).
27. Meredith, E. S. et al. Cities near volcanoes: which cities are most exposed to volcanic hazards? *Nat. Hazards Earth Syst. Sci.* **25**, 2731–2749 (2025).
28. Danesi, S., Pino, N. A., Carlino, S. & Kilburn, C. R. Evolution in unrest processes at Campi Flegrei caldera as inferred from local seismicity. *Earth Planet. Sci. Lett.* **626**, 118530 (2024).
29. Iervolino, I. et al. Seismic risk mitigation at Campi Flegrei in volcanic unrest. *Nat. Commun.* **15**, 10474 (2024).
30. Meredith, E. S. et al. Lava flow impacts on the built environment: insights from a new global dataset. *J. Appl. Volcanol.* **13**, 1 (2024).
31. Smittarello, D. et al. Precursor-free eruption triggered by edifice rupture at Nyiragongo volcano. *Nature* **609**, 83–88 (2022).
32. Baxter, P. J. & Ancia, A. Human Health and Vulnerability in the Nyiragongo Volcano Crisis, Democratic Republic of Congo, 2002: Final Report to the World Health Organization. (2002).
33. Newhall, C. & Punongbayan, A. FIRE and MUD Eruptions and Lahars of Mount Pinatubo, Philippines. http://pubs.usgs.gov/pinatubo/ (1996).
34. De Guzman, E. M. Eruption of Mount Pinatubo in the Philippines in June 1991. Asian Disaster Reduction Center. https://www.adrc.asia/publications/databook/databook2004/02_02_Philippines.pdf (2004).
35. Bankoff, G. Cultures of Coping: Adaptation to Hazard and Living with Disaster in the Philippines. Philippine Sociological Review vol. 51 https://www.jstor.org/stable/44243069 (2003).
36. Intergovernmental Panel on Climate Change (IPCC). Cities, Settlements and Key Infrastructure. In Climate Change 2022 – Impacts, Adaptation and Vulnerability 907–1040 Cambridge University Press. https://doi.org/10.1017/9781009325844.008 (2023).
37. Nirandjan, S., Koks, E. E., Ward, P. J. & Aerts, J. C. A spatially-explicit harmonized global dataset of critical infrastructure. *Sci. Data* **9**, 150 (2022).
38. Strader, S. M., Ashley, W. & Walker, J. Changes in volcanic hazard exposure in the Northwest USA from 1940 to 2100. *Nat. Hazards* **77**, 1365–1392 (2015).
39. Auker, M. R. et al. A statistical analysis of the global historical volcanic fatalities record. http://www.appliedvolc.com/content/2/1/2 (2013).
40. Jenkins, S. F., Magill, C. R. & Blong, R. J. Evaluating relative tephra fall hazard and risk in the Asia-Pacific region. *Geosphere* **14**, 492–509 (2018).
41. Jenkins, S. F. et al. Evaluating and ranking Southeast Asia's exposure to explosive volcanic hazards. *Nat. Hazards Earth Syst. Sci.* **22**, 1233–1265 (2022).
42. Alberico, I., Petrosino, P. & Lirer, L. Volcanic hazard and risk assessment in a multi-source volcanic area: The example of Napoli city (Southern Italy). *Nat. Hazards Earth Syst. Sci.* **11**, 1057–1070 (2011).
43. Thouret, J. C. et al. Geology of El Misti volcano near the city of Arequipa, Peru. *Geol. Soc. Am. Bull.* **113**, 1593–1610 (2001).
44. Magill, C. & Blong, R. Volcanic risk ranking for Auckland, New Zealand. II: Hazard consequences and risk calculation. *Bull. Volcanol.* **67**, 340–349 (2005).
45. Wood, N. & Soulard, C. Variations in population exposure and sensitivity to lahar hazards from Mount Rainier, Washington. *J. Volcanol. Geotherm. Res.* **188**, 367–378 (2009).
46. Newhall, C. & Hoblitt, R. Constructing event trees for volcanic crises. *Bull. Volcanol.* **64**, 3–20 (2002).
47. Ewert, J. W. System for ranking relative threats of U.S. volcanoes. *Nat. Hazards Rev.* **8**, 112–124 (2007).
48. Biass, S. et al. How well do concentric radii approximate population exposure to volcanic hazards? *Bull. Volcanol.* **86**, 3 (2023).
49. Aspinall, W. et al. Volcano hazard and exposure in GFDRR priority countries and risk mitigation measures: GFDRR volcano risk study. (The World Bank, 2011).
50. Brown, S. K., Auker, M. R. & Sparks, R. S. J. Populations around Holocene volcanoes and development of a Population Exposure Index. in Global Volcanic Hazards and Risk (eds Loughlin, S. C., Sparks, R. S. J., Brown, S. K., Jenkins, S. F. & Vye-Brown, C.) 223–232 (Cambridge Univ. Press, 2015).
51. Nieto-Torres, A., Guimaraes, L. F., Bonadonna, C. & Frischknecht, C. A new inclusive volcanic risk ranking, Part 1: Methodology. *Front. Earth Sci.* **9**, 697451 (2021).
52. Jimenez, D., Becerril, L., Carballo, A., Baires, S. & Martí, J. Estimating exposure around San Miguel Volcano, El Salvador. *J. Volcanol. Geotherm. Res.* **386**, 106675 (2019).
53. Major, J., Schilling, S., Sofield, D., Escobar, C. & Pullinger, C. Volcano Hazards in the San Salvador Volcano Hazards in the San

Salvador, El Salvador Region, El Salvador Region, El Salvador. https://pubs.usgs.gov/of/2001/0366/pdf/of2001-0366.pdf (2001).
54. Aravena, A. et al. Scenario-based probabilistic hazard assessment for explosive events at the San Salvador Volcanic complex, El Salvador. *J. Volcanol. Geotherm. Res.* **438**, 107809 (2023).
55. GFDRR. The making of a riskier future: How our decisions are shaping future disaster risk. (Global Facility for Disaster Reduction and Recovery, 2016).
56. Iglesias, V. et al. Risky development: Increasing exposure to natural hazards in the United States. *Earths Future* **9**, e2020EF001795 (2021).
57. Gu, D. Population Division Exposure and Vulnerability to Natural Disasters for World's Cities*. www.unpopulation.org (2019).
58. Guimarães, L. F., Nieto-Torres, A., Bonadonna, C. & Frischknecht, C. A new inclusive volcanic risk ranking, Part 2: Application to Latin America. *Front. Earth Sci.* **9**, 757742 (2021).
59. Ruiz, P. et al. Geomorphological insights on human-volcano interactions and use of volcanic materials in pre-hispanic cultures of Costa Rica through the Holocene. *Front. Earth Sci.* **6**, 13 (2018).
60. UN-Habitat. State of Latin American and Caribbean Cities 2012: Towards a new urban transition. (UN-Habitat, 2012).
61. Meredith, E. S., Handley, H., Jenkins, S. F., Chim, M. M. & Gregg, C. High-impact low-probability events: Exposure to potential large-magnitude explosive volcanic eruptions. Anthropocene in press, 100542 (2026).
62. Smith, V. C. et al. The magnitude and impact of the 431 CE Tierra Blanca Joven eruption of Ilopango, El Salvador. https://doi.org/10.1073/pnas.2003008117/-/DCSupplemental.
63. Silleni, A., Giordano, G., Isaia, R. & Ort, M. H. The magnitude of the 39.8 ka Campanian Ignimbrite eruption, Italy: Method, uncertainties and errors. *Front. Earth Sci.* **8**, 543399 (2020).
64. Hotta, Y., Suzuki, H., Sawai, K. & Tanada, T. Explanatory Volume for the Volcano Hazard Map Collection of Japan, 2nd Edition. http://www.bosai.go.jp/ (2013).
65. Becker, J., Robertson, C. & Johnston, D. M. A Synthesis of Challenges and Opportunities for Reducing Volcanic Risk through Land Use Planning in New Zealand Ministry of Civil Defence and Emergency Management. https://www.researchgate.net/publication/282613375 (2010).
66. Japan Meteorological Agency. Sakurajima hazard map. (Japan Meteorological Agency, 2023).
67. Wilkinson, E. Beyond the volcanic crisis: co-governance of risk in Montserrat. *J. Appl. Volcanol.* **4**, 3 (2015).
68. De Vivo, B. & Rolandi, G. Vesuvius: Volcanic hazard and civil defense. *Rendiconti Lincei* **24**, 39–45 (2013).
69. Becker, J. S., Saunders, W. S. A., Robertson, C. M., Leonard, G. S. & Johnston, D. M. A synthesis of challenges and opportunities for reducing volcanic risk through land use planning in New Zealand. Australas. J. Disaster Trauma Stud. 2010-1 (2010).
70. Douglass, M. Mega-urban regions and world city formation: Globalisation, the economic crisis and urban policy issues in Pacific Asia. *Urban Stud.* **37**, 2315–2335 (2000).
71. Kundu, D. & Pandey, A. K. World urbanisation: trends and patterns. In Developing National Urban Policies: Ways Forward to Green and Smart Cities (eds Kundu, D., Sietchiping, R. & Kinyanjui, M.) 13–49 (Springer Nature Singapore, 2020).
72. Angel, S., Lamson-Hall, P., Blei, A., Shingade, S. & Kumar, S. Densify and expand: A global analysis of recent urban growth. *Sustainability* **13**, 3835 (2021).
73. Güneralp, B., Reba, M., Hales, B. U., Wentz, E. A. & Seto, K. C. Trends in urban land expansion, density, and land transitions from 1970 to 2010: A global synthesis. *Environ. Res. Lett.* **15**, 044015 (2020).
74. Addis Ababa City Administration Environmental Protection Authority. Environment, natural resource degradation & prevention in Addis Ababa. (Addis Ababa City Administration Environmental Protection Authority, 2024).
75. Merrilees, B., Miller, D. & Herington, C. City branding: A facilitating framework for stressed satellite cities. *J. Bus. Res.* **66**, 37–44 (2013).
76. Winarso, H., Hudalah, D. & Firman, T. Peri-urban transformation in the Jakarta metropolitan area. *Habitat. Int.* **49**, 221–229 (2015).
77. Yeung, Y. M. Coastal mega-cities in Asia: transformation, sustainability and management. *Ocean Coast. Manag.* **44**, 319–333 (2001).
78. Jickling, D. L. Increasing responsiveness: Executive power in the Municipality of Guatemala since 1944. Paper prepared for delivery at the 1998 meeting of the Latin American Studies Association, Palmer House Hilton Hotel, Chicago, Illinois, 24–26 September 1998 (1998).
79. Maria, A., Acero, J. L., Aguilero, A. I. & Garcia Lozano, M. Central American Urbanization Review: Making Cities Work for Central America. (World Bank Publications, 2017).
80. Ortiz, D. I., Piche-Ovares, M., Romero-Vega, L. M., Wagman, J. & Troyo, A. The impact of deforestation, urbanization, and changing land use patterns on the ecology of mosquito and tick-borne diseases in Central America. *Insects* **13**, 20 (2021).
81. World Bank. Understanding Migration in North Central America Countries: El Salvador, Guatemala, Honduras and Nicaragua. (2022).
82. United Nations. International Decade for Natural Disaster Reduction. UN General Assembly Resolution A/RES/44/236 (22 December 1989).
83. Annen, C. & Wagner, J.-J. The Impact of Volcanic Eruptions During the 1990s. (2003) https://doi.org/10.1061/ASCE1527-698820034:4169
84. Bastos Moroz, C. & Thieken, A. H. Urban growth and spatial segregation increase disaster risk: Lessons learned from the 2023 disaster on the North Coast of São Paulo, Brazil. *Nat. Hazards Earth Syst. Sci.* **24**, 3299–3314 (2024).
85. Mester, B., Frieler, K., Korup, O., Desai, B. & Schewe, J. Socioeconomic predictors of vulnerability to flood-induced displacement. *Nat. Commun.* **16**, 8296 (2025).
86. World Bank. El Salvador country land assessment. (World Bank, 2012).
87. Alexander Chávez, J. et al. Promoting Resilience and Sustainability in the Metropolitan Area of San Salvador Promoting Resilience and Sustainability in the Metropolitan Area of San Salvador Planning Office of the Metropolitan Area. *Email Address* **3**, 2617–9946 (2020).
88. Mojica Bonilla, A. I. Assessing urban containment policies for managing the urban growth of Santa Tecla City, El Salvador. (Master's thesis, Ohio University 2007).
89. Erfurt-Cooper Editor Geoheritage, P. Volcanic Tourist Destinations. http://www.springer.com/series/11639
90. Newhall, C. G. & Punongbayan, R. S. The narrow margin of successful volcanic-risk mitigation. In Monitoring and mitigation of volcano hazards (eds Scarpa, R. & Tilling, R. I.) 807–838 (Springer, 1996).
91. Donovan, A., Eiser, J. R. & Sparks, R. S. J. Scientists' views about lay perceptions of volcanic hazard and risk. *J. Appl. Volcanol.* **3**, 15 (2014).
92. Loughlin, S. C., Sparks, S., Brown, S. K., Jenkins, S. F. & Vye-Brown, C. Global Volcanic Hazards and Risk. Global Volcanic Hazards and Risk Cambridge University Press (2015). https://doi.org/10.1017/CBO9781316276273.
93. United Nations Office for Disaster Risk Reduction. Sendai Framework for Disaster Risk Reduction 2015–2030. (UNISDR, 2015).
94. Fusinato, E., Han, S., Kobiyama, M. & de Brito, M. M. Safe development paradox: evidence and methodological insights from a systematic review. *Nat. Hazards* **120**, 13693–13714 (2024).

95. Donovan, A. & Oppenheimer, C. Science, policy and place in volcanic disasters: Insights from Montserrat. *Environ. Sci. Policy* **39**, 150–161 (2014).
96. Lavigne, F. et al. People's behaviour in the face of volcanic hazards: Perspectives from Javanese communities, Indonesia. *J. Volcanol. Geotherm. Res.* **172**, 273–287 (2008).
97. Ortiz-Báez, P., Freire, M. J. & Bogaert, J. Analysis of Peri-Urban Landscape composition and its spatio-temporal transformations: the case of the Metropolitan District of Quito. *J. Archit. Urban.* **47**, 1–11 (2023).
98. Lagmay, A. M. F., Bagtasa, G., Crisologo, I. A., Racoma, B. A. B. & David, C. P. C. Volcanoes magnify Metro Manila's southwest monsoon rains and lethal floods. *Front. Earth Sci.* **2**, 36 (2015).
99. Kassa, F. The rates and effects of Urban Sprawl in developing countries: the case of Addis Ababa, Ethiopia. *Int. J. Area Stud.* **9**, 135–151 (2014).
100. Stoler, J., Painter, M. A., Sharygin, E. & Shah, S. H. The rise of hazard gentrification. *Int. J. Disaster Risk Reduct.* **126**, 105618 (2025).
101. Carlino, S. Brief history of volcanic risk in the Neapolitan area (Campania, southern Italy): a critical review. *Nat. Hazards Earth Syst. Sci.* **21**, 3097–3112 (2021).
102. Gomez, C. & Wassmer, P. Evolution du volcan Unzen et de la péninsule de Shimabara (Japon) durant les 60 dernières années: Le rôle de l'éruption de 1990-1995 dans la modification du paysage. Geomorphol.: Relief Process. *Environ.* **21**, 205–216 (2015).
103. Tedesco, D. et al. January 2002 volcano-tectonic eruption of Nyiragongo volcano, Democratic Republic of Congo. *J. Geophys. Res. Solid Earth* **112**, B09202 (2007).
104. Weir, A. M. et al. Quantifying systemic vulnerability of interdependent critical infrastructure networks: A case study for volcanic hazards. *Int. J. Disaster Risk Reduct.* **114**, 104994 (2024).
105. Rustiadi, E. et al. Impact of continuous Jakarta megacity urban expansion on the formation of the Jakarta-Bandung conurbation over the rice farm regions. *Cities* **111**, 103000 (2021).
106. Firman, T. & Dharmapatni, I. A. I. The emergence of extended metropolitan regions in Indonesia: Jabotabek and Bandung Metropolitan Area. *Rev. Urban Reg. Dev. Stud.* **7**, 167–188 (1995).
107. Global Volcanism Program. Report on Fuego (Guatemala). https://doi.org/10.5479/si.GVP.BGVN201808-342090 (2018).
108. Elissondo, M. et al. Chronology and impact of the 2011 Cordón Caulle eruption, Chile. *Nat. Hazards Earth Syst. Sci.* **16**, 675–704 (2016).
109. Mothes, P. A. & Vallance, J. W. Lahars at Cotopaxi and Tungurahua Volcanoes, Ecuador: Highlights from Stratigraphy and Observational Records and Related Downstream Hazards. In Volcanic Hazards, Risks and Disasters 141–168 Elsevier Inc. https://doi.org/10.1016/B978-0-12-396453-3.00006-X (2015).
110. Echegaray-Aveiga, R. C., Rodríguez-Espinosa, F., Toulkeridis, T. & Echegaray-Aveiga, R. D. Possible effects of potential lahars from Cotopaxi volcano on housing market prices. *J. Appl. Volcanol.* **9**, 4 (2020).
111. Suzuki, T. H. istory and future of volcanic disasters in and around the Tokyo Metropolitan Area. *Cent. Jpn. J. Geogr.* **122**, 1088–1098 (2013).
112. Tsunematsu, N., Nagai, T., Murayama, T., Adachi, A. & Murayama, Y. Volcanic ash transport from Mount Asama to the Tokyo metropolitan area influenced by large-scale local wind circulation. *J. Appl. Meteorol. Climatol.* **47**, 1248–1265 (2008).
113. Todde, A., Cioni, R., Pistolesi, M., Geshi, N. & Bonadonna, C. The 1914 Taisho eruption of Sakurajima volcano: stratigraphy and dynamics of the largest explosive event in Japan during the twentieth century. *Bull. Volcanol.* **79**, 72 (2017).
114. Jenkins, S. F. et al. Assessing volcanic hazard and exposure in a data poor context: Case study for Ethiopia, Kenya, and Cabo Verde. *Prog. Disaster Sci.* **23**, 100350 (2024).
115. Global Volcanism Program. Report on Galunggung (Indonesia) (McClelland, L., ed.). Scientific Event Alert Network Bulletin, 7:6. Smithsonian Institution. https://doi.org/10.5479/si.GVP.SEAN198206-263140 (1982).
116. Miyaji, N., Kan'no, A., Kanamaru, T. & Mannen, K. High-resolution reconstruction of the Hoei eruption (AD 1707) of Fuji volcano, Japan. *J. Volcanol. Geotherm. Res.* **207**, 113–129 (2011).
117. Cole, P. D. & Scarpati, C. The 1944 eruption of Vesuvius, Italy: Combining contemporary accounts and field studies for a new volcanological reconstruction. *Geol. Mag.* **147**, 391–415 (2010).
118. Tennant, E. et al. Reconstructing eruptions at a data limited volcano: A case study at Gede (West Java). J. Volcanol. Geotherm. Res. 418 (2021).
119. Balangue-Tarriela, M. I. R. et al. Analysis of the 2020 Taal Volcano tephra fall deposits from crowdsourced information and field data. *Bull. Volcanol.* **84**, 35 (2022).
120. De Risi, R. et al. From flood risk mapping toward reducing vulnerability: the case of Addis Ababa. *Nat. Hazards* **100**, 387–415 (2020).
121. Schiavina, M., Freire, S., Carioli, A. & MacManus, K. GHS POP R2023A – GHS population grid multitemporal (1975–2030). European Commission, Joint Research Centre (JRC) (2023).
122. Schiavina, M., Freire, S., MacManus, K., Pesaresi, M. & Melchiorri, M. GHS UCDB R2023A – Urban Centres Database (1975–2030). European Commission, Joint Research Centre (JRC) (2023).
123. Schiavina, M., Melchiorri, M. & Freire, S. GHS DUC R2023A – GHS Degree of Urbanisation Classification (1975–2030). European Commission, Joint Research Centre (JRC) (2023).
124. Natural Earth. Admin 0 – Countries (1:10 m cultural vectors). Public domain vector dataset. https://www.naturalearthdata.com/ (accessed July 2025).
125. Leyk, S. et al. The spatial allocation of population: a review of large-scale gridded population data products and their fitness for use. *Earth Syst. Sci. Data* **11**, 1385–1409 (2019).
126. Global Volcanism Program. Volcanoes of the World (v. 5.2.7). Smithsonian Institution (2024).
127. Tesema Bulti, D. & Lemmi Eshete, A. Perspective Chapter: Spatio-Temporal Analysis of Urban Expansion. https://doi.org/10.5772/intechopen.107287 (2023).
128. Chen, D., Yang, X., Li, X., Fu, H. & Duan, Y. Quantifying urban land expansion using remote sensing data and multi-evaluation indices in the Lower Yellow River. *China. Environ. Sustain. Indic.* **26**, 100643 (2025).
129. Jenkins, S. F. et al. Volcanic ash fall hazard and risk. in Global Volcanic Hazards and Risk 173–222 (Cambridge University Press, 2015). https://doi.org/10.1017/CBO9781316276273.005.
130. Hersbach, H. et al. The ERA5 global reanalysis. *Q. J. R. Meteorol. Soc* **146**, 1999–2049 (2020).
131. Newhall, C. G. & Self, S. The volcanic explosivity index (VEI) an estimate of explosive magnitude for historical volcanism. *J. Geophys. Res. Oceans* **87**, 1231–1238 (1982).
132. Tennant, E., Jenkins, S. F. & Biass, S. FlowDIR: a MATLAB tool for rapidly and probabilistically forecasting the travel directions of volcanic flows. *J. Appl. Volcanol.* **12**, 10 (2023).
133. OpenStreetMap contributors. OpenStreetMap. https://www.openstreetmap.org (accessed July 2025).
134. Natural Earth. Free vector and raster map data. https://www.naturalearthdata.com (accessed July 2025).
135. European Space Agency. Copernicus Digital Elevation Model (DEM). https://spacedata.copernicus.eu (accessed July 2024).

Acknowledgements

RXNT thanks the volcano colleagues at the Earth Observatory of Singapore for valuable discussions and ideas that helped enhance this work. ESM thanks Hakan Tanyaş for guidance on visualisations, and Marleen de Ruiter for insightful discussions on the work. This research was also partly supported by the Ministry of Education, Singapore, under its MOE Academic Research Fund Tier 3 InVEST project (Award MOE-MOET32021-0002). This work comprises EOS contribution number 670. ESM acknowledges funding from the collaboration of VU Amsterdam-University of Twente, awarded to the impact program Creating Responsible Societies. SFJ acknowledges financial support from the AXA Joint Research Initiative.

Author contributions

E.S.M. and R.X.N.T. conceptualised the project, developed the methodology, and collected and analysed data. E.S.M. produced Figures 2–4 and 8–10 and wrote the first draft of the manuscript. R.X.N.T. produced Figures 1 and 5–7, generated the wind data for the case studies, and developed the visualisation app. For the case studies, E.M.T. generated flow directions. S.F.J., J.L.H., S.B., and D.L. provided conceptual guidance. All authors contributed to the review and editing of the manuscript. E.S.M. and R.X.N.T. contributed equally to this work. All authors have read and approved the manuscript.

Competing interests

The authors declare no competing interests.

Additional information

Supplementary information The online version contains supplementary material available at https://doi.org/10.1038/s44304-026-00203-w.

Correspondence and requests for materials should be addressed to Elinor S. Meredith or Rui Xue Natalie Teng.